

2016

Modelling Hydraulic Fracturing Propagation in Heterogeneous Reservoirs Using Cohesive Zone Methods

Miguel Alejandro Gonzalez-Chavez

Louisiana State University and Agricultural and Mechanical College

Follow this and additional works at: https://digitalcommons.lsu.edu/gradschool_dissertations



Part of the [Petroleum Engineering Commons](#)

Recommended Citation

Gonzalez-Chavez, Miguel Alejandro, "Modelling Hydraulic Fracturing Propagation in Heterogeneous Reservoirs Using Cohesive Zone Methods" (2016). *LSU Doctoral Dissertations*. 2639.

https://digitalcommons.lsu.edu/gradschool_dissertations/2639

This Dissertation is brought to you for free and open access by the Graduate School at LSU Digital Commons. It has been accepted for inclusion in LSU Doctoral Dissertations by an authorized graduate school editor of LSU Digital Commons. For more information, please contact gradetd@lsu.edu.

MODELLING HYDRAULIC FRACTURING PROPAGATION IN HETEROGENEOUS
RESERVOIRS USING COHESIVE ZONE METHODS

A Dissertation

Submitted to the Graduate Faculty of the
Louisiana State University and
Agricultural and Mechanical College
in partial fulfillment of the
requirements for the degree of
Doctor of Philosophy

in

Craft & Hawkins Department of Petroleum Engineering

by

Miguel Alejandro Gonzalez-Chavez

B.S., National Autonomous University of Mexico, 2001

M.S., National Autonomous University of Mexico, 2004

August 2016

©Copyright by Miguel Alejandro Gonzalez-Chavez, 2016
All Rights Reserved

To my grandparents, Guillermo[†] and Micaela[†]

To my mother, Socorro

To my wife, Norma

To my children, Alejandra and Miguel

Acknowledgments

This dissertation could not have been completed without the great support that I have received from so many people over the years. I wish to offer my most genuine thanks to the following people.

My advisor, Dr. Arash Dahi-Taleghani, for his enduring support and guidance on my research in the past years. My committee members: Drs. Thibodeaux, Kam, Antipov, and Flores-Avila for their invaluable contributions and criticisms that have given shape to this work. The Craft & Hawkins department for offering me the opportunity to advance my knowledge and skills through their graduate program. In addition, credit also goes to all members of Geomechanics Research Group at Louisiana State University for their help, support, and friendship during these years. Friends and fellows of LSU for the good moments.

PEMEX E&P and CONACYT for the financial support for this project. Especially to Drs. Pedro Silva and Fernando Flores for all their kindness and support.

My grandparents, Guillermo[†] and Micaela[†], whose I'll always have them in my mind. My mother Socorro, the bravest woman I've ever met; thank you for all her love and support. Norma for accepting to live this adventure together. To my children, Alejandra and Miguel, whose hugs and kisses always gave me the energy to overcome bad days. Family and friends in Mexico for their support.

Last but not least I dedicate this work to God. I thank him for showing me that dreams come true. God's times are perfect.

Table of Contents

Acknowledgments	iv
List of Tables	vii
List of Figures	viii
Abstract	xii
Chapter 1 Overview	1
1.1 Introduction	1
1.2 Research Objectives	4
1.3 Outline	4
1.4 References	5
Chapter 2 Fracture Networks	7
2.1 Introduction	7
2.2 Hydraulic Fracture Process	9
2.3 Evidences of Natural Fractures	11
2.4 Natural Fractures' Interactions with Hydraulic Fractures	12
2.5 Possible Propagation paths of Hydraulic Fracture	14
2.6 Governing Equations	16
2.7 Hydraulic Fracture Modelling	18
2.8 References	21
Chapter 3 Cohesive Zone Method (CZM)	24
3.1 Introduction	24
3.2 Cohesive Zone Method Theory	25
3.3 Implementation in Hydraulic Fracturing	27
3.4 Validation CZM: Single Hydraulic Fracture	32
3.5 Semicircular Bending Test (SCBT)	34
3.6 References	36
Chapter 4 Two-dimensional Hydraulic Fracturing Model	40
4.1 Introduction	40
4.2 Numerical Definition at the Intersection	42
4.3 Validation of CZM: Hydraulic Fracturing Opening in Presence of Natural Fracture	44

4.4	Results.....	46
4.4.1	Case A. Effect of the Natural Cement Strength.....	47
4.4.2	Case B. Natural Cement Ductility	50
4.4.3	Case C. Non-Perpendicular Fracture Intersection	51
4.4.4	Case D: Natural fracture with weak bonding (Factor=0.2)	52
4.4.5	Case E: Natural fractures with strong cement bonds (Factor=1)	54
4.4.6	Case F: Weak cement bonds in the natural fracture (Factor=0.2)	56
4.4.7	Case G: Natural fractures with strong cement bonds (Factor=1)	56
4.4.8	Interaction with multiple natural fractures	57
4.5	References	59
Chapter 5	Three-dimensional Hydraulic Fracturing Model.....	63
5.1	Introduction.....	63
5.2	Numerical Implementation	67
5.3	Validation of CZM: Hydraulic Fracturing 3D model	70
5.4	Results and Discussion	71
5.5	Conclusions.....	76
5.6	References	78
Chapter 6	Conclusions and Recommendations.....	80
6.1	Summary	80
6.2	Recommendations for Future Works	82
	Appendix: Letters of Permission to Use Published Material	84
	Vita	87

List of Tables

3.1	Rock Properties.	33
4.1	Cases analyzed for two-dimensional model.....	48
5.1	Cases analyzed for three-dimensional model.....	72

List of Figures

2.1	Outcrops show a parallel set of natural fractures. Picture was taken close to Chicontepec field in the state of Veracruz, Mexico	12
2.2	Possible scenarios at the normal intersection of a hydraulic fracture and a natural fracture.	14
3.1	Cohesive bilinear law is demonstrated in the above plot for tensile loading. Traction will increase until it reaches T_{max} with an opening of δ_0 , and then traction will decreases until reaches zero traction at δ_f where the cohesive layer is completely damaged.....	26
3.2	Embedded cohesive zone at the tip of a hydraulic fracture. Two zones can be identified: i) broken cohesive zone where traction-separation law is no longer effective, and ii) unbroken cohesive zone where traction-separation law is working.....	28
3.3	Traction-separation for pure tension and pure shear is demonstrated here. Traction increases until it reaches δ_0 , where it is considered that the cohesive layers start to separate. Traction decreases as separation increases to δ_f , where it is considered complete failure. Beyond this, traction-separation law is no longer valid.	30
3.4	Two type of flows inside the fracture: i) tangential flow, which contributes to fracture opening, and ii) normal flow, which is the fluid that will be lost in the formation (better known as leak-off).....	31
3.5	Left picture, a two-dimensional model for single hydraulic fracture. The red line represents the cohesive elements representing the predefined path of the opening of the hydraulic fracture and green elements represent the plane strain for the reservoir. The injection wellbore is at the center of the cohesive layer. Right picture, zoom in view of the cohesive elements.	33
3.6	Left plot, pressure profile along a propagating fracture through the cohesive path at different times. Right plot, fracture opening at the corresponding times is also demonstrated in the bottom graph.....	34

3.7	Semicircular Bending Test. a) Laboratory sketch, b) numerical mesh where the red line represents the cohesive elements	35
3.8	Match results of numerical simulation and lab experiments	35
4.1	Cohesive elements at the tip of a hydraulic fracture are shown above. Two zones can be identified in the fracture: i) broken cohesive zone where traction-separation law is no longer valid, and ii) unbroken cohesive zone.	41
4.2	Sketch of cohesive elements arrangement at the intersection of a growing hydraulic fracture and a pre-existing natural fracture: a) before propagation reaching the intersection point, b) zoom-in of coupling of pressure nodes at the intersection, c) case when fracture crosses over the natural fracture, and d) diversion of the hydraulic fracture into natural fracture.....	42
4.3	Cohesive properties of the formation rock and cemented natural fractures. a) rock with weaker cohesive properties, b) rock with stronger cohesive properties in comparison to the cemented natural fractures	43
4.4	Plot to define whether the opening of the hydraulic fracture will be diverted, crossing or arrested once it reaches a natural fracture based on differential horizontal stress and angle (Blanton, 1982).	44
4.5	Opening when natural fracture path intersects hydraulic fracture with differential horizontal stress field of 1, 2, 3, and 4 MPa. The left picture shows the opening of the hydraulic fracture and the right picture shows the opening of the natural fracture. X-axis at zero mts shows the intersection between the fractures.	45
4.6	Opening when natural fracture path intersects hydraulic fracture at 30, 45, 60, and 90 degrees. The left picture shows opening of hydraulic fracture, and the right picture shows opening of natural fracture. X-axis at zero meters shows the intersection between the fractures.....	46
4.7	Sketch of the model in Abaqus software to simulate the intersection of a hydraulic fracture (horizontal red line) and a natural fracture (vertical red line) for 90 degrees (Left figure) and 45 degrees (Right figure).	46
4.8	Cohesive properties of hydraulic fracture and natural fracture for case A and B.	47
4.9	Perpendicular model, case A with factor 0.2, (a) hydraulic fracture opening, (b) natural fracture opening, (c) pressure propagation along hydraulic fracture path, and (d) pressure propagation along natural fracture path	49
4.10	Perpendicular model, case A with factor 10, (a) hydraulic fracture opening. (b) Pressure profile along hydraulic fracture path.....	49

4.11	Perpendicular model, case B with factor 0.2, (a) hydraulic fracture opening. (b) natural fracture opening, (c) pressure propagation along hydraulic fracture path, (d) pressure propagation along natural fracture path.....	50
4.12	Perpendicular model, case A with factor 0.2, (a) Hydraulic fracture opening, (b) pressure propagation along natural fracture path	51
4.13	Opening (left) and pressure (right) propagates only in the left side of the hydraulic fracture.	51
4.14	The opening profile for Factor=0.2. a) Opening of the hydraulic fracture with intersection point at 40 m. away from the wellbore. b) Opening along the natural fracture	53
4.15	Pressure profile for Factor=0.2. a) hydraulic fracture and b) natural fracture..	53
4.16	a) The opening profile of hydraulic fracture for Factor=1.0. The Presence of natural fracture did not affect the opening in the hydraulic fracture. b) Pressure profile of hydraulic fracture	54
4.17	Bottomhole net pressure is compared when the hydraulic fracture crosses the fracture and when the path is diverted through natural fracture path	54
4.18	Net pressure comparison for different stress fields for sketch a) 45 degrees and b) 90 degrees for different stress fields	56
4.19	Opening profile for the case with Factor=0.2. a) Opening along the original path of the hydraulic fracture. b) The opening of the part of hydraulic fracture expanded along the natural fracture	57
4.20	Computational models built to simulate the propagation of a hydraulic frac- ture in a network of natural fractures are shown above. a) sketch with a spacing of 5 meters between fractures, and b) spacing of 24 meters in the horizontal direction and 16 meters in the vertical direction. The wellbore in both sketches is shown by a black dot in the center.....	58
4.21	Net pressure behavior for: a) sketch with 5 meters spacing among fractures, and b) higher spacing among the fractures	59
5.1	a) Schematic representation of a layered reservoir with natural fractures, where the ideal hydraulic fracture path (red dotted line) is expected to be perpen- dicular to the minimum horizontal stress (σ_2), b) probable hydraulic fracture geometry in the presence of natural fractures, which resembles the situation in the field.	64

5.2	. Selection of the proper zone to perforate need to take in account interlayering of the rock at wellbore level and continuity of these layers through the reservoir. Left picture show gamma ray log intercalation of sandstone and shale. Right picture shows seismic and cross section of an unconventional reservoir basin with pinch-outs and discontinuities in Mexico.	65
5.3	Sketch of cohesive elements arrangement at the intersection of a growing hydraulic fracture (orange path) and a pre-existing natural fracture (blue path). Zoom figure shows the share pressure nodes to assure the fluid flow continuity.	68
5.4	: Numerical sketch or the reservoir (green elements) and the path of the two cracks (red lines).	69
5.5	Schematic representation of three-dimensional model of one hydraulic fracture path (orange) that is intersected by a natural fracture at 30 degree (blue). Yellow zone represents lower or higher cohesive rock properties in the hydraulic fracture path (yellow). Injection point is 10 meters away of the intersection of the fractures and five meters away the beginning of the plug zone.....	70
5.6	Comparison of half fracture length shows that analytical solution (Equation 5.1) gives higher fracture length than numerical model using cohesive elements.	71
5.7	Net pressure response for the hydraulic fracture diverting into natural fractures: 1) when weaker layer case is in the natural fracture, and 2) when tougher layer case is in the middle layer of hydraulic fracture path.....	72
5.8	Case 1. Opening of hydraulic and natural fracture due presences of weak (upper figure) and tougher (bottom figure) layer on the middle layer of hydraulic fracture path.	73
5.9	Case 2. Net pressure response when Tougher/weaker layer is in the middle layer. Weaker layer case shows extra net pressure drop and Tougher layer case shows faster propagation in the other direction.....	74
5.10	Case 2. Opening of hydraulic and natural fractures due presence of weak layer (upper figure) and tough (bottom figure) layer on the 2- and 4-layer of hydraulic fracture path.	74
5.11	Case 3. Net pressure response when tougher/weaker layer is 4- and 5- layer. Weak layer shows lower net pressure drop and tough layer shows faster propagation in the other direction.	75
5.12	Case 3. Opening of hydraulic and natural fractures due presence of weaker (upper figure) and tougher (bottom figure) layer on the 4- and 5-layer of hydraulic fracture path.	76

Abstract

The recent success in exploiting low permeability shale reservoirs has heavily relied on hydraulic fracturing to produce hydrocarbons economically in disadvantaged reservoir conditions. Although horizontal drilling significantly increases the contact area between the wellbore and the reservoir, the objective of hydraulic fracturing is set on creating further expanded conductive flow paths into the reservoir.

This research uses cohesive zone method to numerically simulate hydraulic fracture propagation in the presence of natural fractures in two- and three-dimensional model. The Cohesive element approach limits fracture propagation to some predefined paths. However, in highly fractured formations since hydraulic fractures are growing through a network of natural fracture by placing cohesive elements through natural fractures it is possible to track the development of a network of induced hydraulic fractures. Moreover, cohesive elements remove stress singularity at the tips of fractures, which improves numerical stability of the model. Additionally, fracture models based on Griffith's criterion cannot predict fracture initiation. A numerical model was developed coupling both fluid flow in fracture network and rock deformations to study the interaction between hydraulic and natural fractures at different scales. The cohesive zone method assumes the existence of a fracture process zone characterized by a traction-separation law rather than an elastic crack tip region. The cohesive finite element method provides an alternate, effective approach for quantitative analysis of fracture behavior through explicit simulation of the fracture process.

Activation of natural fractures during fracturing treatment improves the effectiveness of the stimulation tremendously. Here, integrated methodology initiated with laboratory-scale fracturing properties using a semicircular bending test is presented to determine cohesive properties of rock and natural fractures. A cohesive finite element model is used to reproduce laboratory results to verify the numerical model for interaction between the hydraulic fracture and cemented natural fractures. The results suggest that the distribution of pre-existing natural fractures can play a significant role in the final geometry of the induced fracture network. Moreover, understanding of natural fracture distribution in the reservoir will have an economical impact in projects where fracture geometry is better designed according to underground conditions.

Chapter 1

Overview

1.1 Introduction

Large quantities of hydrocarbons have been discovered in very low permeability formations around the world. Hydraulic fracturing is recognized as the only technique to make production economic in these formations (Holditch, 2006). However, hydraulic fracturing has not been a successful treatment everywhere due to different geological or petrophysical situations. The main objective in hydraulic fracturing is to create a crack with high fluid flow conductivity to maximize well productivity by increasing the wellbore formation contact area.

Some parameters can be controlled in designing a typical fracturing. The controllable parameters include jobs such as injection rate, fracturing fluid rheology, volume of injected fluid, proppant size and pumping schedule. On the other hand, major parameters such as permeability, closure pressure, tectonic stress anisotropy, and geological effects like faults and fractures are out of our control. Although a few parameters could be measured directly in the laboratory or estimated using logs, other parameters cannot be measured directly. Additionally, limited access to the subsurface makes fracture geometry and other properties of the formations like distribution of natural fractures unknown to us. These restrictions limit fracturing assessments limited to production data. However, modeling fracturing treatment and honoring measured treatment data may provide a tool to estimate fracture parameters and improving fracture design by virtual numerical experiments.

Fractures are present in every formation (Narr et al., 2006). The size and abundance of natural fractures determine the potential influence of natural fractures on hydraulic fracturing treatments. Acquired microseismic data in the fields (Waters *et al.*, 2006) has shown that presence of natural fractures in some cases has led to the formation of a network of induced fractures rather than a single symmetric bi-wing hydraulic fracture. Dahi (2009) built a two-dimensional model using eXtended Fracture Elastic Mechanics (XFEM) and demonstrated how complex fracture pattern could affect the fracture geometry. He also determined whether the geometry of the hydraulic fracture will be affected or not due the presence of natural fracture network, depending on how they are oriented towards and/or intersecting the hydraulic fracture. Different techniques have been used to describe the characteristic behavior of induced fracture networks based on treatment data like bottomhole pressure and injection rate. Some of these methods, such as the volume of stimulate rock (Cipolla et al., 2008), mainly provide overall properties. Other methods, like wiremesh (Xu et al., 2010), are more well transient analysis conditioned to microseismic events locations, rather considering the fracturing process.

Modeling of fractures is generally classified to analytical and numerical categories. Analytical solutions are limited to simple fracture geometries placed in homogeneous isotropic formations. For most situations, there is no closed form solution for the propagation of fluid driven fractures. On the other hand, the numerical simulation can be used to obtain solutions for more complex problems. Many numerical techniques have been used to simulate the propagation of hydraulic fractures such Distinct Element Methods, Boundary Element Methods, and Finite Element Methods. In this research, I plan to use the cohesive element approach to simulate fracture propagation in three-dimensional geometries. Cohesive element approach limits fracture propagation to some predefined paths. However, in highly fractured formations, since hydraulic fractures are growing through a network of natural fracture by placing cohesive elements through natural fractures, it is possible to track the development of a network of induced hydraulic fractures. Moreover, cohesive elements re-

move stress singularity at the tips of fractures, which improves the numerical stability of the model. Additionally, fracture models based on Griffith's criterion cannot predict fracture initiation, which can be investigated using the cohesive element approach.

To study the interaction between hydraulic fracture and natural fractures at different scales, a three-dimensional model with the capability of coupling fluid flow in fracture network and rock deformations should be considered. The cohesive zone model assumes the existence of a fracture process zone characterized by a traction-separation law rather than an elastic crack tip region. The cohesive finite element method provides an alternate, effective approach for quantitative analysis of fracture behavior through explicit simulation of the fracture process. The presence of the fissures will be modeled using cohesive elements.

This document presents an integrated cohesive model to analyze hydraulic fracturing jobs in the presence of a natural fracture network. A propagating hydraulic fracture may arrest, cross, or divert into a pre-existing natural fracture depending on the fracture properties of the rock, magnitude and direction of principal rock stresses, and the angle between fractures. Activation of natural fractures during fracturing treatment improves the effectiveness of the stimulation tremendously. Here, integrated methodology initiated with lab-scale fracturing properties using a semicircular bending test (SCBT) is presented to determine cohesive properties of rock and natural fractures. A cohesive finite element model is used to reproduce laboratory results to verify the numerical model for interaction between the hydraulic fracture and cemented natural fractures. The hydraulic fractures' growth in the reservoir scale is then simulated, in which the effect of fluid viscosity, natural fracture characteristics, and differential stresses on induced fracture network is studied. The results suggest that the distribution of pre-existing natural fractures could play a significant role in the final geometry of the induced fracture network.

1.2 Research Objectives

The proposed research has the following objectives:

- Build a two-dimensional hydraulic fracture model using the cohesive interface technique for modeling radial and KGD fracture propagation. This model will act a benchmark for three-dimensional models, which will be developed in the next stages of this research.
- Develop the two-dimensional model to a three-dimensional hydraulic fracture model; the new model gives me the opportunity to investigate the growth of hydraulic fractures in heterogeneous reservoirs. Asymmetric fracture growth and non-uniform height growth are the main characteristics that will be incorporated into the model at this stage.
- Model interaction of the propagating hydraulic fracture with short-height pre-existing natural fractures and investigate how the distribution of natural fractures may impact the geometry of induced fracture networks. The model will consider the interaction between natural fractures of different sizes and orientations, and the hydraulic fracture during well stimulation treatments.

1.3 Outline

This dissertation is concerned with two main topics: validation of cohesive input parameters to represent the rock properties of the shale for a sample found in the literature, and perform a numerical simulation to validate those cohesive elements representing hydraulic fracture in two- and three-dimensional models.

In Chapter 2, hydraulic fracture process is explained. A literature review of how natural fractures interact with hydraulic fracture jobs is presented. Review of governing equations

in hydraulic fractures modeling and summary of principal techniques of hydraulic fracturing will be discussed.

In Chapter 3, the theory of cohesive zone model (CZM) is reviewed and how it will be implemented in hydraulic fracturing. Validation of CZM for single hydraulic fracture is provided. Semicircular bending test is used to obtain cohesive parameters that will be used in two- and three-dimensional models in the following chapters.

In Chapter 4, a review of modeling of the hydraulic fracture in the presence of natural fractures in a two-dimensional model is presented. Validation of whether the hydraulic fracture propagation is crossed, diverted or arrested by the presence of natural fractures is shown. Different cases for interaction between hydraulic fracture and natural fractures are discussed.

In Chapter 5, a three-dimensional model is used and validated. Several cases were analyzed based on changes of rock properties of the fracture paths.

Finally, Chapter 6 summarizes the main results in this dissertation and gives recommendations for future works.

1.4 References

- Charlez, P. A., 1997, Rock Mechanics, Volume 2. Petroleum Applications. Editions Technip.
- Cipolla, C.L., Warpinski, N.R., and Mayerhofer, M., 2008, The Relationship between Fracture Complexity Reservoir Properties and Fracture Treatment Design, Society of Petroleum Engineers.
- Dahi Taleghani, A., 2009, Analysis of hydraulic fracture propagation in fractured reservoirs: an improved model for the interaction between induced and natural fractures.
- Dahi Taleghani, A. and Olson, J.E., 2011, Numerical Modeling of Multistranded-Hydraulic-Fracture Propagation: Accounting for the Interaction between Induced and Natural Fractures (in SPE Journal 16 (03): 575-581.
- Dahi Taleghani, A., Puyang, P., Le Calvez, J. and Lorenzo, J., 2013, Post-Treatment Assessment of Induced Fracture Networks, SPE-166354-MS presented in SPE Annual Technical Conference and Exhibition in New Orleans, LA, USA.

- Gale, J.L.W., Reed, R.M. and Holder, J., 2007, Natural Fractures in the Barnett Shale and Their Importance for Hydraulic Fracture Treatments (in AAPG bulletin 91 (4): 603-622.
- Holditch, S.A., 2006, Tight Gas Sands (in Journal of Petroleum Technology 58) (6): 86-93.
- Jeffrey, R.G., Zhang, X. and Thiercelin, M.J., 2009, Hydraulic Fracture Offsetting in Naturally Fractured Reservoirs: Quantifying a Long-Recognized Process, Society of Petroleum Engineers.
- Laubach, S. E., 2003, Practical approaches to identifying sealed and open fractures: AAPG Bulletin, v. 87, p. 561579, doi:10.1306 /11060201106.
- Narr, W., Schechter, D.W. and Thompson, L.B., 2006, Naturally fractured reservoir characterization. Richardson, TX: Society of Petroleum Engineers.
- Ortega, O. J., Marrett, R., and Laubach, S. E., 2006, A scale-independent approach to fracture intensity and average fracture spacing: AAPG Bulletin, v. 90, no. 2 (Feb. 2006), 193-208.
- Potluri, N.K., 2005, The Effect of Natural Fractures on Hydraulic Fracture Propagation (in SPE European Formation Damage Conference).
- Shakib, J. T., Ghaderi, A., and Shahri, A. A., 2012, Analysis of hydraulic fracturing in fractured reservoir: interaction between hydraulic fracture and natural fractures. Life Science Journal, 9(4).
- Warpinski, N.R. and Teufel, L.W., 1987, Influence of Geologic Discontinuities on Hydraulic Fracture Propagation (includes associated papers 17011 and 17074) (in Journal of Petroleum Technology 39 (02): 209-220.
- Waters, G. A., Heinze, J. R., Jackson, R., Ketter, A. A., Daniels, J. L., and Bentley, D., 2006, Use of horizontal well image tools to optimize Barnett Shale reservoir exploitation. Society of Petroleum Engineers.
- Xu, W., Thiercelin, M.J., Ganguly, U., Weng, X., Gu, H., Onda, H., Sun, J. and Le Calvez, J., 2010, Wiremesh: A novel shale fracturing simulator. In International Oil and Gas Conference and Exhibition in China. Society of Petroleum Engineers.
- Zhang, X. and Jeffrey, R.G., 2008, Reinitiation or Termination of Fluid Driven Fractures at Frictional Bedding Interfaces (in Journal of Geophysical Research: Solid Earth (19782012) 113 (B8).

Chapter 2

Fracture Networks

2.1 Introduction

In the past few years, improvements in hydraulic fracturing technology contributed significantly to the spikes in gas production in the United States by creating conductive flow paths from the reservoir to the wellbore (USEIA report, 2009). Production from unconventional shale gas reservoirs has relied heavily on this technology. As such, research efforts now center on how to achieve the optimal fracture design with known reservoir characteristics, or at least improve fracturing treatment design. The preliminary step in assessing any hydraulic fracturing job is identifying the geometry of induced fractures. Accurate prediction of the fracture network geometry is a desirable objective, however, rarely accomplished with modern fracturing technology. A model that is able to predict the geometry and evolution pattern of every individual fracture in the fracture network barely exists because it is practically impossible to collect every detail regarding individual fractures. It is also notable that although natural fractures may exist in a wide range of length and widths (Ortega *et al.*, 2006), here, natural fractures comparable in size with hydraulic fractures are of interest. Small natural fractures may also open due to thermal stresses (Dahi-Taleghani *et al.*, 2013a) or residual plastic deformations (Dahi-Taleghani *et al.*, 2013b). Because small fractures will not affect the direction of fracture propagation, here, small natural fractures will be ignored although they can affect the initial hydrocarbon production rate. Therefore, objective is set to develop an optimal approach to describe the seemingly unmanageable spatio-temporal

evolution of fracture patterns. While traditional models assume simple symmetric wing or bi-wing type fracture networks as commonly appropriate for ideal homogeneous reservoirs, they are inadequate in representing the complex nature of the fracture network in reservoirs with pre-existing natural fractures.

Historically, pressure diagnostics (Nolte and Smith, 1979, Nolte, 1991) and tiltmeter measurements (Warpinski *et al.*, 1997) were the main tools for estimating fractures' geometry. Initial steps in pressure analysis include pressure data collection and processing; important information about the formation, fracture and treatment may be obtained by identifying general pressure variation patterns, which are similar to methods used in pressure transient analysis. Economides and Nolte (2004) have provided a complete review of classic pressure diagnostic techniques to infer critical parameters of the fracturing treatment, including fracture geometry, closure pressure, fracture height growth, formation pressure capacity, treatment efficiency, and fluid flow patterns. This approach has gained its popularity in the early 1990's because pressure data is the least costly piece of information to collect in the field, and this method was providing acceptable predictions for massive fracturing jobs in a vertical well. Utilization of hydraulic fracturing to stimulate new developments in low permeability, naturally fractured formations like Barnett shale, which was frequently done in multiple stages through horizontal wells, posed new challenges in interpreting treatment pressure data. With the introduction of hydraulic fracturing into shale plays, which were usually naturally fractured, interactions between natural fractures and hydraulic fractures lead to the formation of a complicated network of induced fractures.

Interactions between hydraulic and natural fractures have been investigated through laboratory experiments. Results have shown that different parameters, especially differential stress, govern the interactions between natural and hydraulic fractures (Warpinski and Teufel, 1987). Further laboratory investigations confirmed the formation of complicated fracture networks in the presence of natural fractures. Jeffrey (2009) conducted mineback field experiments to examine the growth of hydraulic fractures through a system of natural

fractures. In such situations, the induced fracture tends to develop in a much-complicated way due to the diversion of progressing hydraulic fracture into natural fractures, or simply the opening of these fractures (Warpinski and Teufel, 1987, Olson and Dahi-Taleghani, 2004, Dahi-Taleghani and Olson, 2013). This complexity can either be suppressed or utilized to some extent to benefit the reservoir productivity (Cipolla *et al.*, 2008). Considering the fact that all pressure diagnostic techniques were built by considering induced hydraulic fractures as a single-strand fracture, it is not reliable to interpret pressure data of a network of fractures.

Cipolla *et al.* (2008) discussed how fracture network complexity may change bottomhole pressure during the treatment as well as future production in comparison to the cases with single induced fracture. Through reservoir simulation, they claimed that fracture conductivity required to maximize production was proportional to the square root of the fracture spacing. Thus, fracture complexity is inversely proportional to the fracture conductivity requirement. Moreover, they argued that in complicated fracture networks, the average proppant concentration will become insignificant and therefore proppant placement is less likely to impact the wellbore performance. Fluid pressure and injection rate have been used for a long time to estimate fracture geometries. However, due to the complex geometry of induced fracture networks, these methods are not applicable in reservoirs with pre-existing natural fractures.

2.2 Hydraulic Fracture Process

Hydraulic fracturing has been identified as an essential technique to achieve economic production in low-permeability reservoirs (Holditch, 2006). Large quantities of unconventional hydrocarbon resources have been discovered in very low permeability formations around the world (Rogner, 1997). Understanding how hydraulic fracture geometry will be developed in the presence of natural fractures might help to design more efficient stimulations in these formations. The main objective in hydraulic fracturing treatments is to create a fracture

with high flow conductivity inside the tight rock to enhance production by increasing the wellbore-formation contact area. However, the injected volume during a fracturing treatment may not completely contribute to creating new hydraulic fractures because a part of the injected volume may be diverted into the pre-existing natural fractures. Fractures are present in every formation (Narr and Thompson, 2006). The size and abundance of natural fractures determine the potential influence of natural fractures on hydraulic fracturing treatments. Extensive field studies have revealed the presence of natural fractures in different length scales. Hence, interactions between hydraulic and natural fractures may occur in different scales. Small scale natural fractures or microfractures may not change the direction of hydraulic fracture propagation at all; however, they can still increase well formation contact area (Dahi-Taleghani *et al.*, 2013).

Injection rate, fracturing fluid rheology, the volume of injected fluid, proppant size, and pumping schedule are parameters that can be controlled during a hydraulic fracturing job. On the other hand, major parameters, such as closure pressure, tectonic stress anisotropy, rock toughness and geological effects like faults and fractures, are dictated by formation properties. However, only some of such parameters can be measured directly in the laboratory or estimated using logs. Additionally, limited access to the subsurface makes an estimation of natural fracture geometry impossible. Hence, a robust modeling tool can be extremely helpful to examine numerous realizations of natural fractures to find the most probable configuration that honors measured treatment data in the field (Dahi-Taleghani *et al.*, 2013). Current industry practices in assessing and modeling hydraulic fracturing treatments relied on simplified fracture and fluid flow models, which would only provide approximated estimations regarding the actual fracture geometry. For instance, common assumptions in fracturing modeling include homogeneous formation properties and fracture growth in a symmetric double-wing fashion. These common assumptions are likely to be erroneous in unconventional gas reservoirs where material properties and fracture development can be quite complicated (Valencia *et al.*, 2005).

2.3 Evidences of Natural Fractures

Outcrops (Seeburger and Zoback, 1982, Hennings *et al.*, 2000, Ortega *et al.*, 2006) as well as core studies (Gale *et al.*, 2007) have revealed the presence of considerable natural fractures in some low permeability unconventional formations like Mesa Verde formation (Lorenz and Sharon, 1989) and Barnett Shale (Gale *et al.*, 2007, Jarvie *et al.*, 2007). Figure 2.1 shows outcrops of Mexican oil field with very tight permeability. While production analyses have confirmed the potential role of natural fractures, there is no systematic tool for simulating fracture propagation in these reservoirs. For the case of Barnett Shale, natural fractures are mostly sealed with calcite and quartz coming from mineralized water from the underlying Ellenburger limestone formation. The lack of open natural fractures actually leads to the formation of the reservoir by preventing gas migration to upper formations and precluded overpressurized reservoir conditions observed today (Bowker, 2007). Cemented fracture zones are believed to enhance hydraulic fracturing by acting as preferential weak paths for the deflection of induced fractures, and can result in a more complex fracture network. Initially, operators targeted highly fractured zones and thought that faulted zones would have higher permeability and fracture porosity. However, better production outcomes are reported for wells outside of fault zones because within the fault zones, induced hydraulic fractures develop along fault planes and lead into the underlying water-bearing Ellenburger. Hence, the presence of pre-existing natural fractures is not always advantageous if the treatment design is not considering this fact (Hopkins *et al.*, 1998). Unfortunately, due to the limited access to the subsurface, monitoring the interaction between hydraulic and natural fractures cannot be done by direct observation. Even widely used techniques, such as microseismic, may only show the effect of natural fractures on hydraulic fracture growth qualitatively but not quantitatively because of their inherent uncertainties (Le Calvez *et al.*, 2006, Dahi-Taleghani and Lorenzo, 2011).



Figure 2.1: Outcrops show a parallel set of natural fractures. Picture was taken close to Chicontepec field in the state of Veracruz, Mexico

2.4 Natural Fractures' Interactions with Hydraulic Fractures

In general, tight sandstones, coal bed methane, and shale formation may contain natural fractures. Because of the low permeability of these formations and the low conductivity of the natural fracture networks, stimulation treatments are crucial to achieving economic production. The low hydraulic conductivity of the natural fractures could be caused by cements that precipitated during the diagenesis process (Laubach, 2003). The fact that natural fractures might be occluded by cement materials does not mean that they can be ignored while designing well stimulation. Cemented natural fractures may act as weak paths for fracture growth (Gale *et al.*, 2007, Dahi-Taleghani and Olson, 2011).

Efforts to understand this problem are not limited to field observations and mathematical modeling. Lab experiments were also performed to reproduce field data and examine mathematical models. Lamont and Jessen (1963) performed 70 hydraulic fracturing experiments in six different rock types using triaxial compression with different approaching angles to understand the fracture crossing phenomenon. The size of their samples was less than a meter. Hydraulic fractures appeared to crossover closed pre-existing fractures at all in-

tersection angles. However, Lamont and Jessen noted that the fracture propagation speeds in their experiments were considerably greater than those of field tests due to the lack of correct scaling, making their results less reliable. Daneshy (1974), based on his experiments, was one of the first to argue that the hydraulic fractures appeared to be arrested when the natural fractures were open at the intersection and appeared to cross the natural fractures when they were closed. Later, Hanson *et al.* (2000) showed the importance of friction on hydraulic fracture growth near unbonded interfaces in rock. These tests were performed in Nugget sandstone and Indiana Limestone under uniaxial loading. The results lead to the formulation of a threshold of normal stress below which fracture is arrested by a natural fracture. They found that this normal stress is inversely proportional to friction between surfaces of the natural fracture. Cleary *et al.* (1991) argued that fracture energy, due to its internal pressure, is high enough to open any fracture in any orientation, but they did not give any clear scheme or analysis for their claim. Later, field observations in Marcellus shale proved that only a subset of natural fractures, depending on their orientation, main fracture geometry, and other parameters, can be opened and contribute to hydrocarbon production. Warpinski and Teufel (1987), Jeffrey *et al.* (2009), and Cipolla *et al.* (2008) indicated that the pressure behaviors during fracture treatment will be affected by the presence of fracture networks. The sudden change of fracture propagation direction due to its deflection into natural fractures may also show its effect as high frequency events in microseismic data. However, this data may not be used for quantitative analysis due to the inherent uncertainty in locating the events, because of the large wavelength of microseismic waves (Dahi-Taleghani and Lorenzo, 2011).

Zhang and Jeffrey (2008) used two-dimensional boundary element simulation and found that large modulus or toughness contrast among the cracks can lead to containment of the hydraulic fracture on the interface. They also argued that offsetting could happen when one of the layers has lower critical tensile stress similar to far interaction mechanism between hydraulic fracture and natural fractures (Dahi-Taleghani and Olson, 2013).

2.5 Possible Propagation paths of Hydraulic Fracture

Three possibilities might occur during the hydraulic fracturing of naturally fractured reservoirs (Figure 2.2). First, the natural fractures may have no influence at all, and the hydraulic fracture will propagate in a direction parallel to the maximum horizontal stress as expected in the classic sense. This may be a result of high cement strength in the natural fractures (comparable to matrix strength), unfavorable natural fractures orientation, or a fracturing pressure that is not high enough to overcome the normal stress perpendicular to the natural fracture. In the second scenario, once the hydraulic fracture intersects the natural fracture, the hydraulic fracture is arrested, and the fluid is completely diverted into the natural fracture system. The natural fractures will open if the energy of the growing hydraulic fracture is large enough to debond (re-open) fracture cements or if the shear stresses are large enough to overcome the friction between fracture surfaces. In the third scenario, both the newly formed hydraulic fracture and the natural fractures will interact and intersect in a complex manner. The mode of opening will depend on the angle between hydraulic fracture and natural fracture, stresses, infilling material, and fluid properties.

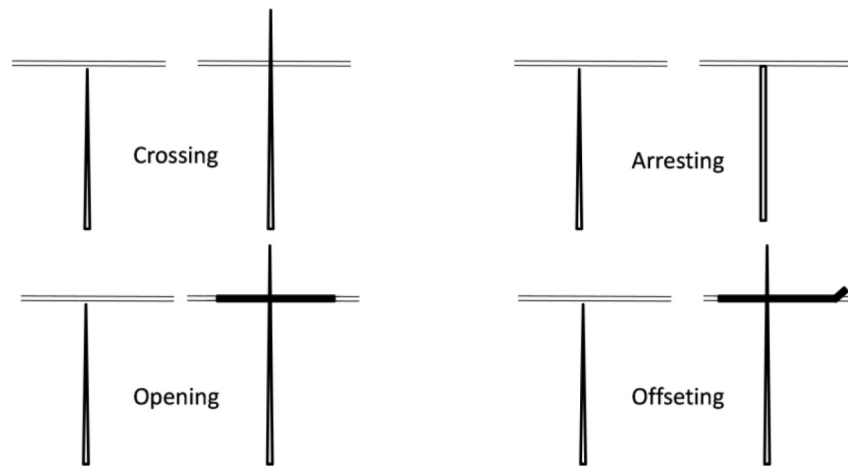


Figure 2.2: Possible scenarios at the normal intersection of a hydraulic fracture and a natural fracture.

Jeffrey *et al.* (1987) used two-dimensional displacement discontinuity methods for investigating the interaction between natural fractures and hydraulic fractures. They were able to model slippage along the hydraulic fracture due to the presence of natural fractures. Akulich and Zvyagin (2008) investigated the interaction between a growing hydraulic fracture and a fault in an infinite impermeable elastic medium under plane strain conditions. They considered incompressible Newtonian fluid for the fracturing fluid and the Mohr-Coulomb criterion for fault failure. For fluid flow inside the hydraulic fracture, they assumed zero net pressure at the front as the boundary condition. Their modeling did not indicate fracture intersections; however, it gave an idea about the slippage along the fault and how it affected the stress intensity factors at the tip of the growing hydraulic fractures. Later, Olson and Dahi-Taleghani (2009) argued that hydraulic fractures will grow in the direction with maximum energy release rate, which was a suitable case for cemented natural fractures as toughness could be easily defined and measured along these fractures. However, in most geological settings, numerous fractures with various sizes exist, and their interactions in different scales dictate fracture growth pattern at the intersection with natural fractures.

The size of natural fractures ranges from a few millimeters (tiny fissures) to several thousand meters (faults). As opposed to natural fractures, hydraulic fractures are created artificially with the force of injected pressurized fluid. By generating a hydrostatic pressure that exceeds the minimum in-situ stress of the formation, fractures are opened up in a direction perpendicular to that of smallest resistance, i.e., minimum principal stress.

Improved hydrocarbon production does not necessarily rely on hydraulic fracturing. In some cases, natural fractures may also contribute to the recovery of oil and gas. Natural fractures in formations with moderate permeability can serve as the flow path for hydrocarbons as well, and the presence of natural fractures may facilitate the formation of a network of induced fractures. On the other hand, natural fractures may also negatively impact hydraulic fracturing treatment by causing extensive leak-off and reduced flow back (Warpinski, 1990); a large population of natural fractures in the subsurface is cemented by diagenetic materials.

Although they will not increase overall permeability initially, the opening of these natural fractures will increase drainage area tremendously. Fortunately, in most cases, these natural fractures act as weak paths for fracture growth. Therefore, if they are aligned in a favorable direction with in-situ tectonic stresses, there is a good likelihood that these natural fractures can be opened during treatment (Gale *et al.*, 2007, Dahi-Taleghani and Olson, 2013). The intersections of natural fractures with hydraulic fractures result in irregular fracture patterns, including non-planar fractures or fracture branching. On one hand, the opening of these natural fractures improves the productivity of the formation; on the other hand, coalescence of these fractures into hydraulic fractures makes pressure analysis and prediction of fracture growth quite complicated. Overall, interactions between natural fractures and hydraulic fractures make the fracturing design and execution more challenging. Investigation and understanding of their interaction are crucial in achieving successful fracture treatment in formations with natural fracture network.

2.6 Governing Equations

Hydraulic fracturing consists of pumping viscous fluid at high rates, increasing the pressure at the formation until the rock breaks and the fluid continues flowing through the crack and further expanding the crack. Considering the fact that the largest principal stress is in the vertical direction, the hydraulic fracture will be vertical and will propagate perpendicular to the minimum horizontal stress field. Hence, we limited our analysis to two-dimensional plane strain analysis to avoid excessive computational costs while the expansion of the proposed methodology to three dimensions is straightforward. The physical process mentioned above involves coupling equations for fluid flow, rock deformation, and fracture propagation. We consider rock as a porous medium. Porous media deformation that relates total stresses, bulk strains, and pore pressure is given as (Rice and Cleary, 1976)

$$\sigma_{ij} - \sigma_{ij}^0 = \frac{E}{1 + \nu}(\varepsilon_{ij} + \frac{\nu}{1 - 2\nu}\varepsilon_{kk}\delta_{ij}) - \alpha(p - p_0)\delta_{ij}, \quad (2.1)$$

where repeated indices imply summation. $\sigma_{ij}, \sigma_{ij}^0, E, \nu, \varepsilon_{ij}, p, p_0$, and α are stress components, initial stress components, Young's Modulus, Poisson's ratio, strain tensor, pore fluid pressure, initial pore pressure, and Biot's constant, respectively. Here, K and G are the bulk and shear modulus respectively.

The fluid flow inside the fracture can be presented by the lubrication equation (Batchelor, 1967)

$$q = -\frac{w^3}{12\mu} \nabla p_f, \quad (2.2)$$

where $q, w, \mu, \nabla p_f$ represent the pumping rate, fracture width, viscosity of the pumping fluid, and pressure gradient, respectively. This equation assumes that fluid rate inside the fracture is directly proportional to both the injection pressure gradient and fractures width (w) and inversely proportional to the injected fluid viscosity. Injected fluid is considered to be incompressible. The fluid mass balance states that a part of the pumping fluid volume at a specific time, fills the fracture and the other part will be lost to the formation as shown in the following equation

$$\frac{\partial w}{\partial t} + \nabla \cdot q + (q_t + q_b) = Q(t)\delta(x, y) \quad (2.3)$$

where q_t and q_b are the normal fluid loss rate in the top and bottom face of the formations respectively, q is the mass flow rate along the fracture, and Q is the total volume pump at the specific time.

The equations presented in this section describe displacement and stress distributions, but these equations do not predict fracture initiation and subsequent propagation. Fractures may form whenever stress in any part of the material exceeds its strength, which could be shear stress, normal stress, or both. The most common method of modeling fracture propagation is the Griffith's criterion; however, this criterion can only predict the propagation of pre-

existing fractures, not their initiation. In the next chapter, a cohesive interface approach is used to fill this gap. Description of this approach is provided in the next section.

Fracture propagation in fracture mechanics is a function of opening and shearing mode stress intensity factors, which measure stress concentration at the tip of the crack (Lawn, 2004). The two stress intensity factors are combined in the energy release rate based fracture propagation criterion used in this research. The energy release rate, G , is related to the stress intensity factors through Irwin's relation (Lawn, 2004). In the case that enough energy is available for fracture propagation and the crack has more than one path to follow (Figure 2.2), its most likely path is one with the maximum energy release rate, or the greater relative energy release rate (Dahi-Taleghani and Olson, 2013). The details of energy criterion and its implementation can be found in Dahi-Taleghani and Olson (2013).

2.7 Hydraulic Fracture Modelling

Modeling of fractures is generally classified into analytical and numerical categories. Analytical solutions (for instance Detourany, 2004) are limited to simple fracture geometries in homogeneous, isotropic formations. In most situations, there is no closed form solution for the propagation of fluid driven fractures. On the other hand, the numerical simulation could obtain solutions for more complex problems. Many numerical techniques have been used to simulate the propagation of hydraulic fractures such as Distinct Element Methods, Boundary Element Methods, and Finite Element Methods. In all of these models, force equilibrium and elasticity relations to govern deformations of the rock, and the fluid flow inside the fracture is idealized as flow down a slot using lubrication theory (Batchelor, 1967).

Dahi-Taleghani (2009) used an Extended Finite Element Method (XFEM) to address two-dimensional static and quasi-static problems. Crack propagation in strong and weak quasi-static form was described by deriving the governing equations from XFEM. By decomposing the displacement field into continuous and discontinuous parts, XFEM can approximate the behavior of hydraulic fractures and their interactions with natural fractures

in a naturally fractured reservoir, without any need for remeshing the problem for each increment of fracture propagation. Dahi-Taleghani and Olson (2013) extended the numerical analysis of hydraulic fracture/natural fracture interaction to the case of cemented natural fractures. These fractures can influence the geometric development of hydraulic fractures, which consequently affects the resulting gas production. They examined different scenarios of fracture interactions using an eXtended Finite Element Method (XFEM) numerical scheme that considers the fluid flow in hydraulic fracture networks as well as the rock deformation.

Different numerical techniques have been proposed to simulate the propagation of hydraulic fractures in the last three decades. For instance, Wilson and Witherspoon (1974) used Boundary Element Method (BEM) to simulate the steady state flow in rigid networks of planar fractures. Shapiro and Andersson (1983) and Cleary and Wong (1985) used displacement discontinuity BEM for modeling penny-shaped hydraulic fractures. Iwashita and Oda (2000) used a modified version of DEM (MDEM) to investigate micro-deformation of granular media to deal with rolling resistance of the blocks at contact points. Finite Element Methods (FEM) was used by Martha *et al.* (1993), Carter *et al.* (2000), and Bouchard *et al.* (2000) to model fractures' growth utilizing various remeshing strategies. Advani *et al.* (1990) modeled three-dimensional planar hydraulic fractures in a multi-layered medium. Considering the need for remeshing at each step of fracture propagation in finite element models, Extend Finite Element Method (XFEM) was used to address this deficiency by letting fractures pass through the elements without any requirement for mesh refinement (Dahi-Taleghani and Olson, 2011). They set a criterion for fracture diversion based on the fracture energy of both natural and hydraulic fracture and the orientation with respect to each other. In parallel to this revision in FEM, Cohesive Zone Method (CZM) was used by Chen *et al.* (2009) to simulate hydraulic fracture propagation in the penny-shape model. Later, Sarris and Papanastasiou (2011a) simulated hydraulic fracture simulation in a plane strain reservoir in elastic and poroelastic materials.

Here, the cohesive interface approach is used to simulate fracture propagation in three-dimensional geometries. Cohesive element approach limits the fracture propagation to pre-defined paths. In highly fractured formations, since hydraulic fractures are growing through a network of natural fractures by placing cohesive elements through natural fractures, it is possible to track potential paths in the development of a network of induced hydraulic fractures. Inserting cohesive properties at the tip of the fracture removes stress singularity at the said tips, which improves the numerical stability of the model.

To study the interaction between hydraulic fracture and natural fractures with different heights, a three-dimensional model is required to incorporate interactions and coalescence of fractures with different sizes. The cohesive zone model assumes the existence of a fracture process zone characterized by a traction-separation law rather than an elastic crack tip region. The cohesive finite element method provides an effective alternative approach for quantitative analysis of fracture behavior through explicit simulation of the fracture process. The presence of fissures will be modeled using cohesive elements.

Numerical models discussed above assume that the geometry of natural fractures is given. Due to limited access to the subsurface to monitor fractures, simulation of natural fractures has always been considered as an option to predict fracture growth in the subsurface (Olson, 2004). Any hydraulic fracturing simulation is generally built upon existing formation and fracture properties, including formation geomechanical properties, treatment, and petrophysical data, as well as the exact location of natural fractures. However, the location and dimension of natural fractures cannot be determined accurately using seismic or logging tools. This limitation has restricted the application of commercial and academic fracturing simulators. Several approaches have been taken in the industry to address this deficiency. In the first approach, a fully random set of fractures is considered as consisting of natural fractures, and hydraulic fracture is assumed only to propagate through these fractures (Meyer and Bazan, 2011), which does not completely represent the actual fracture distribution in the formation of interest. Extensive outcrop studies in the last couple of decades demonstrate

that joints distribution is not a fully random distribution; depending on the rock properties and tectonic history, it may range from a single set of parallel joints to multiple sets of intersecting joints (Ortega and Marret, 2000, Ortega *et al.*, 2006). Additionally, depending on formation properties, each joint set can be equally spaced or clustered (Olson and Dahi-Taleghani, 2004). In summary, the pattern of induced fracture networks is dictated by natural fractures and their orientation with respect to principal in-situ stresses. Therefore, we need to set our goal to speculate the characteristic geometry of natural fractures in the subsurface, rather than take a deterministic approach to determining the exact location of each fracture as this problem is ill-conditioned and does not have a unique solution.

Any non-deterministic approach requires acquiring a forward model to simulate hydraulic fracture propagation for different realizations of natural fractures. Therefore, it is expected that the forward model to be quick enough to include numerous natural fracture realizations, capable of modeling the true mechanics of hydraulic fracture and natural fractures intersections, and model different natural fracture geometries with least costly meshing techniques. It is found cohesive element approach a suitable tool for this technique.

2.8 References

- Bame, D., and M. Fehler, 1986, Observations of long period earthquakes accompanying hydraulic fracturing, *Geophysical Research Letters*, 13(2), 149-152.
- Batchelor, G. K., 1967, *An introduction to fluid dynamics*, Cambridge University Press, Cambridge, UK.
- Cipolla, C.L., Warpinski, N. R., Mayerhofer, M. J., and Lolon, E., 2008, The Relationship Between Fracture Complexity, Reservoir Properties, and Fracture-Treatment Design, Paper SPE 115769, SPE Annual Technical Conference and Exhibition, Denver, Colorado.
- Dahi Taleghani, A., 2009, *Analysis of Hydraulic Fracture Propagation in Fractured Reservoirs : an Improved Model for the Interaction Between Induced and Natural Fractures*, PhD Dissertation, the University of Texas at Austin, Austin, Texas.
- Dahi Taleghani, A. and J.M. Lorenzo, 2011, An Alternative Interpretation of Microseismic Events during Hydraulic Fracturing SPE 140468-PP, presentation at the SPE Hydraulic Fracturing Technology Conference and Exhibition held in The Woodlands, Texas.

- Dahi-Taleghani, A., J. E. Olson, and W. Wang, 2013a, Thermal Reactivation of Microfractures and its potential impact on Hydraulic Fractures Efficiency, SPE-163872-PP, presented at 2013 SPE Hydraulic Fracturing Technology Conference to be held 4-6 February, 2013 in The Woodlands, TX, USA.
- Dahi-Taleghani A., M. Ahmadi and J.E. Olson, 2013b, Secondary Fractures and Their Potential Impacts on Hydraulic Fractures Efficiency, chapter in Effective and Sustainable Hydraulic Fracturing edited by Robert Jeffrey, published by InTech ISBN 980-953-307-651-0.
- Dahi Taleghani, A., and J. Olson, 2013, How Natural Fractures Could Affect Hydraulic Fracture Geometry, Accepted for publication in SPE Journal.
- Economides, M., and Nolte, K., 2000, Reservoir Stimulation, Third Edition, Sugarland, Texas.
- Fehler, M., L. House, and H. Kaieda, 1987, Determining planes along which earthquakes occur: Method and application to earthquakes accompanying hydraulic fracturing, Journal of Geophysical Research: Solid Earth 92(B9): 9407-9414.
- Gale, J.F.W., Reed, R.M. and Holder, J., 2007, Natural fractures in the Barnett Shale and their importance for hydraulic fracture treatments, AAPG Bulletin; v. 91; no. 4; p. 603-622.
- Gilman, J.R. and Kazemi, H., 1988, Improved calculations for Viscous and Gravity displacement in matrix blocks in dual-porosity simulators, J. Pet. Tech, 60-70 (Jan. 1988).
- Jeffrey, R.G., Bunger, A., Lecampion, B., Zhang, X., Chen, Z., van As, A., Allison, D.P., De Beer, W., Dudley, J.W., Siebrits, E. and Thiercelin, M.J., 2009, Measuring hydraulic fracture growth in naturally fractured rock. In SPE Annual Technical Conference and Exhibition. Society of Petroleum Engineers.
- Lawn, B., 2004, Fracture of Brittle Solids, Cambridge University Press.
- Lewis, R. W., and Schreffler B. A., 2000, The finite element method in the static and dynamic deformation and consolidation of porous media. Wiley, London.
- Li, Y., Cheng, C. H., and Toksoz, M. N. 1998, Seismic monitoring of the growth of a hydraulic fracture zone at Fenton Hill, New Mexico, Geophysics, vol. 63, NO. 1, P. 120131.
- Mandl, G., 2005, Rock joints: the mechanical genesis, Springer.
- Maxwell, S.C., 2008, Microseismic location uncertainty, CSEG Recorder.
- Meyer, B. and Bazan, L., 2011, A Discrete Fracture Network Model for Hydraulically Induced Fractures-Theory, Parametric and Case Studies. SPE Hydraulic Fracturing Technology Conference.
- Nolte, K.G. and Smith, M.B., 1979, Interpretation of Fracturing Pressures, Paper SPE 8297 presented at the SPE Annual Technical Conference and Exhibition, Las Vegas, Nevada.

- Nolte, K., 1991, Fracturing-pressure analysis for nonideal behavior, *Journal of Petroleum Technology* 43.2, pp 210-218.
- Olson, J.E., 2004, Predicting fracture swarms the influence of subcritical crack growth and the crack-tip process zone on joint spacing in rocks, in initiation, propagation and arrest of joints and other fractures, Geological society of London Special publication 231, pages: 73-87.
- Olson J. and Dahi-Taleghani A., 2009, Modeling simultaneous growth of multiple hydraulic fractures and their interaction with natural fractures, 2009 SPE 119739, Hydraulic Fracturing Technology Conference.
- Ortega, O., and Marrett, R., 2000, Prediction of macrofracture properties using microfracture information, Mesaverde Group sandstones, San Juan basin, New Mexico. *Journal of Structural Geology*, v. 22(5), pp. 571-588.
- Ortega, O. J., Marrett, R., and Laubach, S. E., 2006, A scale-independent approach to fracture intensity and average fracture spacing: *AAPG Bulletin*, v. 90, no. 2 (Feb. 2006), 193-208.
- Rutledge, J.T., and Phillips, W.S., 2002, A Comparison of Microseismicity Induced By Gel-proppant- And Water-injected Hydraulic Fractures, Carthage Cotton Valley Gas Field, East Texas, Paper SEG 2002-2393 presented at the 2002 SEG Annual Meeting, Salt Lake City, Utah.
- Sarris, E., and Papanastasiou, P., 2012, Modeling of Hydraulic Fracturing in a Poroelastic Cohesive Formation. *International Journal of Geomechanics*, 12(2), 160-167.
- US Energy information Administration report, 2009, Summary: US Crude Oil, Natural Gas, and Natural Gas Liquids Proved Reserves 2009.
- Warpinski, N.R. and Teufel, L.W., 1987, Influence of geologic discontinuities on hydraulic fracture propagation, *Journal of Petroleum Technology*, page: 209220.
- Warpinski, N.R., 1990, Dual leakoff behavior in hydraulic fracturing of tight lenticular gas sands, SPE 18259.
- Warpinski, N. R., Branagan, P. T., Engler, B. P., Wilmer, R., and Wolhart, S. L., 1997, Evaluation of a downhole tiltmeter array for monitoring hydraulic fractures. *International Journal of Rock Mechanics and Mining Sciences*, 34(3), 108-e1.
- Waters, G., Heinze, J., Jackson, R., Ketter, A., Daniels, J. and D. Bentley, 2006, Use of Horizontal Well Image Tools to Optimize Barnett Shale Reservoir Exploitation, SPE 103202, presented at the SPE Annual Technical Conference.
- Xu, W., Thiercelin, M.J., Ganguly, U., Weng, X., Gu, H., Onda, H., Sun, J. and Le Calvez, J., 2010, Wiremesh: A novel shale fracturing simulator. In *International Oil and Gas Conference and Exhibition in China*. Society of Petroleum Engineers.

Chapter 3

Cohesive Zone Method (CZM)*

3.1 Introduction

Linear Elastic Fracture Mechanics (LEFM) (Atkinson and Meredith, 1987) has been very successful in describing fracture behaviors in brittle rocks. However, the success story did not repeat in the soft rock. Considering the fact that an extensive number of hydraulic fracturing treatments are nowadays conducted in soft shale rocks and many brittle rocks may show ductile behavior under high temperature, high pressure conditions in the subsurface, LEFM may not be the best tool to deal with these problems. Additionally, problems like nucleation of cracks cannot be treated directly in LEFM. LEFM neglects the details in the fracture process zone as it lumps all effects into the fracture tip stress singularity; however, a detailed description of the fracture process zone may be essential, especially to understand fracture mechanisms along the intersections or heterogeneous interfaces. In these situations, the size of the fracture process zone is larger than the fracture grain size, which violates the fundamental assumption of LEFM. From this point of view, an efficient tool for fracture studies that allows us to overcome these limitations can be found in the Cohesive Zone Model (CZM). By means of CZM, fracture initiation and growth are obtained as a natural part of the solution. So far, CZM has also been successfully applied to fractures in metals, concrete,

*Part of this chapter 3 previously appeared as "Gonzalez-Chavez, M. A., Dahi-Taleghani, A., and Olson, J. E., 2015, A Cohesive Model for Modeling Hydraulic Fractures in Naturally Fractured Formations. Society of Petroleum Engineers." and "Gonzalez-Chavez, M. A., Puyang, P., and Dahi-Taleghani, A., 2015, From Semi-Circular Bending Test to Microseismic Maps: An Integrated Modeling Approach to Incorporate Natural Fracture Effects on Hydraulic Fracturing. Society of Petroleum Engineers.". There are reprinted by permission of Society of Petroleum Engineers (Appendix A).

polymers and functionally graded materials. Cohesive element theory assumes that the fracture process zone is characterized by a traction-separation law. The presence of cohesive tractions close to the fracture tips removes singularity at the fracture tip while this singularity greatly affects the mathematical solution of the partial differential equations derived from LEFM. As a tradeoff, cohesive tractions make the constitutive equations nonlinear. The standard model used to describe the fracture tip process zone assumes bonds stretching orthogonal to the fracture surfaces until they break at a characteristic stress level. Thus, the singular region introduced from LEFM can be replaced by a zone over which nonlinear phenomena occur. This model is evolved from the Dugdale-Barenblatt process zone (Barenblatt, 1962, Dugdale, 1960). According to CZM, the fracture process is lumped into the fracture line and is characterized by a cohesive law that relates tractions and displacement jump across cohesive surfaces ($T-\delta$). Therefore, the rock is characterized by two constitutive laws a linear stress-strain relationship for the bulk matrix and a cohesive surface relationship (cohesive law) that allows spontaneous fracture initiation and growth in the matrix or along the natural fracture. It is important to properly select the shape of the softening curve; Elices *et al.* (2002) pointed out the advantages, limitations and challenges of CZM; among the more important advantages, CZM is able to predict the fracture behavior in unfractured structures even in ductile metals or for cementitious materials, whereas LEFM cannot predict fracture behavior in those kinds of materials. The CZM possesses several limitations, one of which is the direction of fracture propagation must be known. Additionally, cohesive parameters are obtained for a specific material in laboratory experiments such as a Brazilian test or a semicircular bending test. Literature usually reports experiments with concrete and cement samples. Experiments with shale samples are not common.

3.2 Cohesive Zone Method Theory

The simplest traction-separation model is the bilinear model shown in Figure 3.1. Due to the simplicity of this model and the fact that it is honoring experimental data satisfactorily,

the cohesive model is built based on the bilinear relationships. As traction increases, the separation of the cohesive layers will increase linearly till the traction reaches the maximum tensile strength (T_{max}) at critical separation (δ_0), better known as damage initiation. Beyond this point, the traction will decrease with further separation of fracture surfaces till it reaches complete damage corresponding to the failure opening (δ_f), which is the point the fracture starts propagating. The area below the traction-separation curve is known as cohesive energy (G_c) and the slope of the initial loading curve is known as initial cohesive stiffness (K_n).

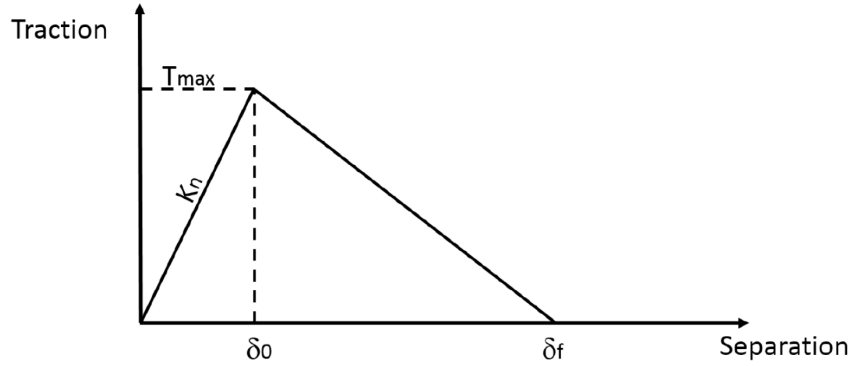


Figure 3.1: Cohesive bilinear law is demonstrated in the above plot for tensile loading. Traction will increase until it reaches T_{max} with an opening of δ_0 , and then traction will decrease until it reaches zero traction at δ_f where the cohesive layer is completely damaged.

Damage initiation is defined by maximum nominal stress (Equation 3.1) and damage propagation is defined by fracture energy (Equation 3.2).

$$T_{max} = K_n \cdot \delta_0 \quad (3.1)$$

$$G_c = \frac{T_{max} \cdot \delta_f}{2} \quad (3.2)$$

Conceptually, fracture initiation can be defined by δ_0 or T_{max} and the fracture propagation by δ_f or G_c . The cohesive interface is introduced as a layer of elements with zero thickness to

predict initiation and growth of a possible fracture. It is notable that due to the importance of fluid pressure in the development of the failure zone, a coupled fluid flow and deformation model has been incorporated in the cohesive elements. Moreover, the model is considered large enough to avoid any potential interference with boundaries. The fracture process zone (unbroken cohesive zone) is defined within the separating surfaces where the surface tractions are nonzero (Figure 3.1). There are three failure mechanisms present during the opening of fractures in the cohesive zone, i) fracture initiation criterion, which is referred to as the beginning of degradation due to the stresses and/or strains satisfies damage initiation criteria; ii) fracture evolution - fracture will propagate when the stress intensity factor at the tip is higher than the rock toughness, and iii) when the cohesive element is completely damaged - beyond this point, the cohesive element no longer exists. The cohesive element approach removes stress singularity at the fracture tips that improves the numerical stability of the model. Additionally, fracture models based on Griffith's criterion cannot really predict fracture initiation, which is possible in the cohesive element approach.

3.3 Implementation in Hydraulic Fracturing

Cohesive zone model assumes the existence of a fracture zone characterized by a traction-separation law. The pre-defined surface is made up of elements that support the cohesive zone traction-opening calculation embedded in the rock, and the hydraulic fracture will grow along this surface. The fracture process zone (unbroken cohesive zone) is defined within the separating surfaces where the surface tractions are nonzero (see Figure 3.2).

There are three failure mechanisms taken into account in fracture modeling: i) fracture initiation criterion, ii) fracture evolution law, and iii) choice of element removal upon reaching a completely damaged state. Fracture Initiation Criterion is referred to as the beginning of degradation due to stresses, and/or strains that satisfy certain damage initiation criteria that were specified. There are many fracture initiation criteria in ABAQUS. It is assumed that initiation begins when maximum nominal, quadratic stress ratio, maximum nominal

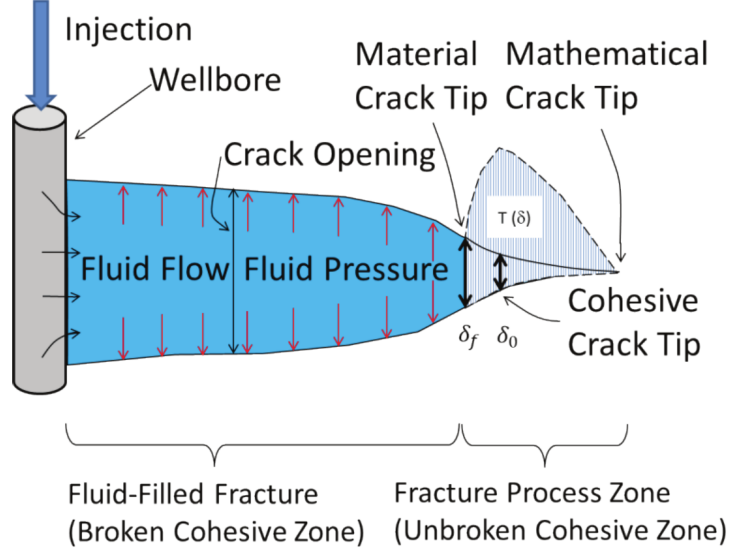


Figure 3.2: Embedded cohesive zone at the tip of a hydraulic fracture. Two zones can be identified: i) broken cohesive zone where traction-separation law is no longer effective, and ii) unbroken cohesive zone where traction-separation law is working.

strain, or quadratic strains reaches its critical value. Fracture Evolution Law Criterion states that the fracture propagates when the stress intensity factor at the tip exceeds the rock toughness. When the interface thickness is negligibly small, it may be straightforward to define the constitutive response of the cohesive layer directly in terms of traction versus separation.

The relationship among G_c , K_n , T_{max} , δ_0 , and δ_f can be described as

$$G_c = \frac{1}{2}T_{max} * \delta_f = \frac{1}{2\alpha}T_{max} * \delta_0 = \frac{T_{max}^2}{2\alpha K} \quad (3.3)$$

where G_c is the cohesive energy, T_{max} is the cohesive strength, K_n is the initial cohesive stiffness, δ_0 and δ_f are the critical separation at damage initiation and complete failure respectively, and α is the ratio of critical separation at damage initiation and complete failure.

Since bilinear traction-separation laws are defined for pure normal and shear loading modes, general loading conditions that can be any arbitrary combinations of normal and shear failure (mixed mode problem) require considering the combined effect of normal and shear modes. The quadratic nominal stress law is used to combine different failure modes. Damage is said to commence when a quadratic interaction function involving nominal stress ratios (as defined below) reaches the value of one (Camacho and Ortiz, 1996)

$$\left\{ \frac{\langle t_n \rangle}{t_{n0}} \right\}^2 + \left\{ \frac{t_s}{t_{s0}} \right\}^2 + \left\{ \frac{t_t}{t_{t0}} \right\}^2 = 1 \quad (3.4)$$

where t_n , t_s , and t_t represents the real values of normal and tangential (first and second shear) traction across the interface, respectively. $\langle \rangle$ is the Macaulay bracket and

$$\langle t_n \rangle = \begin{cases} t_n, & t_n \geq 0 \quad (\text{tension}), \\ 0, & t_n < 0 \quad (\text{compression}) \end{cases} \quad (3.5)$$

The metrics for damage is a scalar stiffness degradation index, D , which represents the overall damage of the interface caused by all stress components. The stiffness degradation index is a function of the so-called effective relative displacement, δ_m by combining the effects of δ_t , δ_s , and δ_n ,

$$\delta_m = \sqrt{\langle \delta_n \rangle^2 + \delta_s^2 + \delta_t^2} \quad (3.6)$$

For linear softening, the damage evolves with the index (Mei et al., 2010)

$$D = \frac{\delta_{mf}(\delta_{m,max} - \delta_{m,0})}{\delta_{m,max}(\delta_{mf} - \delta_{m,0})} \quad (3.7)$$

where $\delta_{m,max}$ is the maximum effective relative displacement attained during loading history. δ_{m0} and δ_{mf} are effective relative displacements corresponding to δ_{n0} and δ_{s0} , δ_{nf} and δ_{sf} are shown in Figure 3.3.

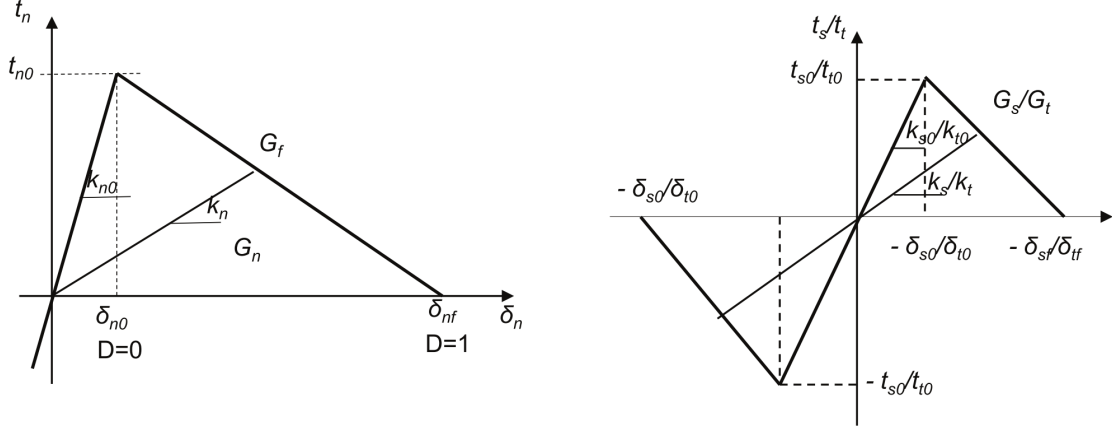


Figure 3.3: Traction-separation for pure tension and pure shear is demonstrated here. Traction increases until it reaches δ_0 , where it is considered that the cohesive layers start to separate. Traction decreases as separation increase to δ_f , where it is considered complete failure. Beyond this, traction-separation law is no longer valid.

For nonlinear mechanics, the most robust criterion is described by the constitutive model of the cohesive zone proposed by Barenblatt (1962) and Hillerborg (1976). This law assumes that the cohesive surfaces are intact without any relative displacement, and exhibit reversible linear elastic behavior until the traction reaches the cohesive strength or equivalently the separation exceeds δ_0 . Beyond this value, the traction reduces linearly to zero up to δ_f . Figure 3.4 shows how crack openings provide paths for tangential and normal flow inside the fracture. The fluid leakoff is the normal flow. The tangential flow within the gap is governed by the lubrication equation (Batchelor, 1967), which is a combination of Poiseuille's flow

$$q = -\frac{w^3}{12\mu} \nabla p_f \quad (3.8)$$

and the continuity equation

$$\frac{\partial w}{\partial t} + \nabla \cdot q + (q_t + q_b) = Q(t)\delta(x, y) \quad (3.9)$$

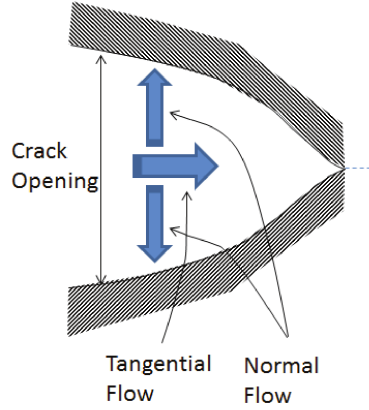


Figure 3.4: Two type of flows inside the fracture: i) tangential flow, which contributes to fracture opening, and ii) normal flow, which is the fluid that will be lost in the formation (better known as leak-off).

In the above equation, $q(x, y, t)$ is the fluid flux in tangential direction, $\nabla p_f(x, y, t)$ is the fluid pressure gradient along the cohesive zone, $w(x, y, t)$ is the crack opening, μ is the viscosity, and $Q(t)$ are fluid viscosity and injection rate, respectively. The $q_t(x, y, t)$ and $q_b(x, y, t)$ terms are the normal flow rates into the top and bottom surfaces of the cohesive elements, respectively. The normal flow rate is defined as

$$\begin{aligned} q_t &= c_t(p_f - p_t) \\ q_b &= c_b(p_f - p_b) \end{aligned} \quad (3.10)$$

where p_t and p_b are the pore pressures in the adjacent pore-fluid (poroelastic) material on the top and bottom surfaces of the fracture, respectively, and c_t and c_b define the corresponding fluid leak-off coefficients. This problem can be approximated numerically using

standard Galerkin formulation for Finite element methods (Lewis and Schreffler, 2000). The equation in matrix notation can be written as the following:

$$\begin{aligned} [K]\{u\} + [L]\{u\} &= \{F\} \\ [S]\{p\} + [L]^T\{u\} + [H]\{p\} &= \{q\} \end{aligned} \tag{3.11}$$

where u are nodal displacements, p are nodal pressures, F are nodal forces, q are nodal fluxes, $[K]$ is the stiffness matrix, $[L]$ is the coupling matrix, $[H]$ is the flow matrix and $[S]$ is the compressibility matrix. The first equation of equations (10) is the stiffness equation and the second equation is the flow equation. Unknown variables u and p are substituted by their nodal values and the interpolation functions (shape functions). The definition of matrices used in equation (10) are given below (Lewis and Schreffler, 2000).

$$\begin{aligned} [K] &= \int_{\Omega} B^T D B \, d\Omega, \\ [L] &= \int_{\Omega} N^u \begin{Bmatrix} d/dx \\ d/dy \end{Bmatrix} N^p \, d\Omega, \\ [S] &= a \int_{\Omega} (N^p)^T \frac{1}{\tilde{Q}} N^p \, d\Omega \\ [H] &= \kappa \int_{\Omega} N^u \begin{Bmatrix} d/dx \\ d/dy \end{Bmatrix} N^p \, d\Omega, \end{aligned} \tag{3.12}$$

where D is the elasticity matrix, N^p and N^u are the shape functions for pressure and displacements, respectively. The parameter \tilde{Q} is defined as $\tilde{Q} = \frac{BK}{\alpha(1-\alpha B)}$.

3.4 Validation CZM: Single Hydraulic Fracture

A two-dimensional finite element model is built in ABAQUS for a single fracture to validate the numerical model. The reservoir size is assumed to be much larger than the dimension of hydraulic fracture and is modeled with quadratic plane strain elements. Injection well is

considered to be at the center of the model, and a layer of cohesive elements passes through the injection well, which represents the possible path for the hydraulic fracture and consists of 6-node cohesive elements. The initial length of the hydraulic fracture, 22 m (Figure 3.5), is set to be much smaller than the model size to avoid any boundary effect.

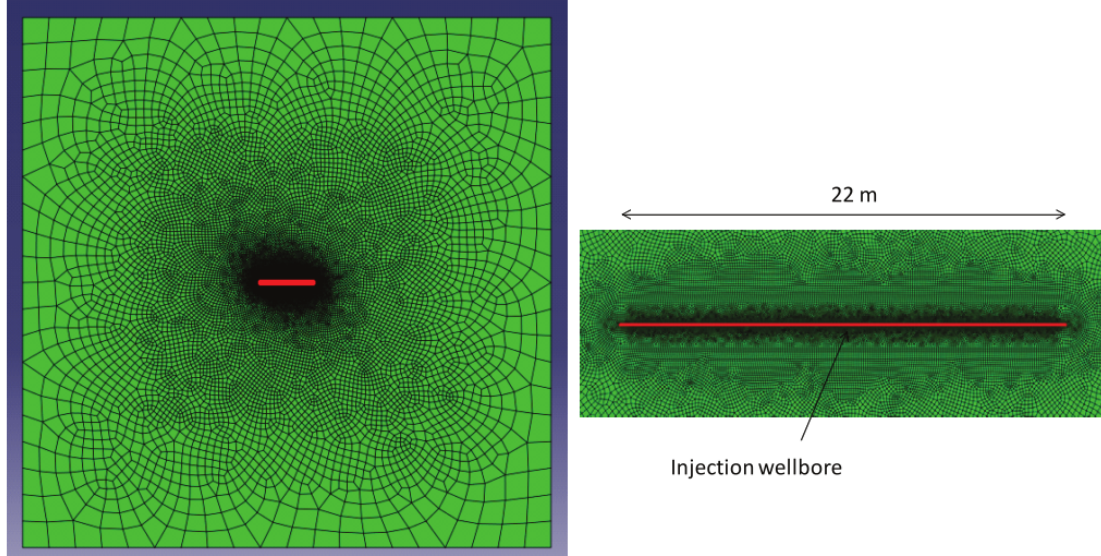


Figure 3.5: Left picture, a two-dimensional model for single hydraulic fracture. The red line represents the cohesive elements representing the predefined path of the opening of the hydraulic fracture and green elements represent the plane strain for the reservoir. The injection wellbore is at the center of the cohesive layer. Right picture, zoom in view of the cohesive elements.

The right and left faces are constrained in the x-direction, and the upper and lower faces were constrained in the y-direction as boundary conditions. The in-situ stresses are defined as initial stresses to avoid any excessive deformation in the initial equilibrium process. The mechanical properties utilized to build this model are listed in Table 3.1. The crack opening displacement profile and fluid pressure profile are demonstrated in Figure 3.6, which are similar to the results reported previously by Sarris and Papanastasiou (2012).

Table 3.1: Rock Properties.

$E(GPa)$	ν	$\mu(cp)$	$q(m^3/sec * m)$	$T_{max}(MPa)$	$K_n(GPa)$	$G_c(Pa * m)$
15	0.2	1	200e-6	2.46	80	100

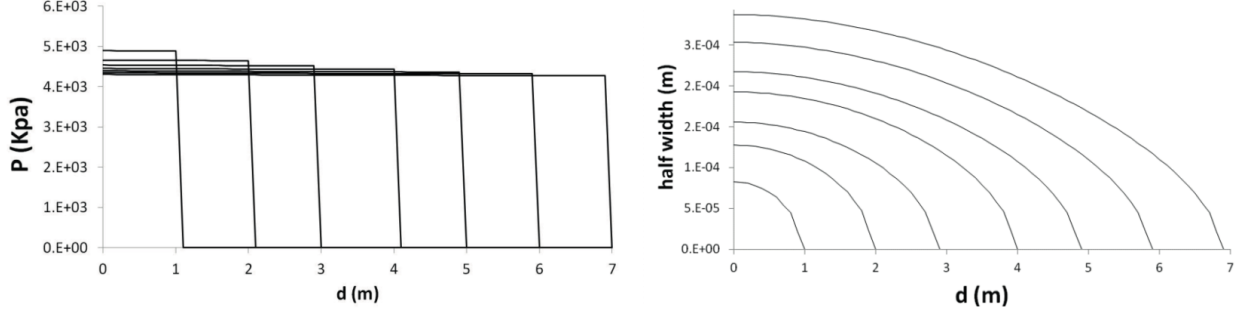


Figure 3.6: Left plot, pressure profile along a propagating fracture through the cohesive path at different times. Right plot, fracture opening at the corresponding times is also demonstrated in the bottom graph.

3.5 Semicircular Bending Test (SCBT)

Extensive laboratory studies have shown that the inherently nonlinear nature of interfacial fractures in granular materials can be better described by cohesive zone models. The main challenge in using cohesive models is choosing, or being more precise, is measuring cohesive model parameters in the lab. Semicircular Bending Test (SCBT) is a laboratory experiment that determines when the rock will fail when under a certain applied force. The load versus displacement plot obtained is useful to obtain cohesive parameters. It uses finite element numerical results inversely to determine cohesive stiffness, strength and energy properties. Cohesive properties are calibrated such that the simulated test results match the measured response of the specimens.

Sierra *et al.* (2010) performed SCBT test for several shale rock samples (Figure 3.7,a). Cohesive parameters (Table 3.1) were obtained matching the load versus displacement plot (Figure 3.8) from numerical simulation (Gonzalez *et al.*, 2015) (Figure 3.7,b).

Cohesive parameters seem to match reasonably as the equivalent fracture toughness for mode I is approximately 1.25 MPa , according to equation 3.13.

$$K_{IC} = \sqrt{E' \cdot G_c} \quad (3.13)$$

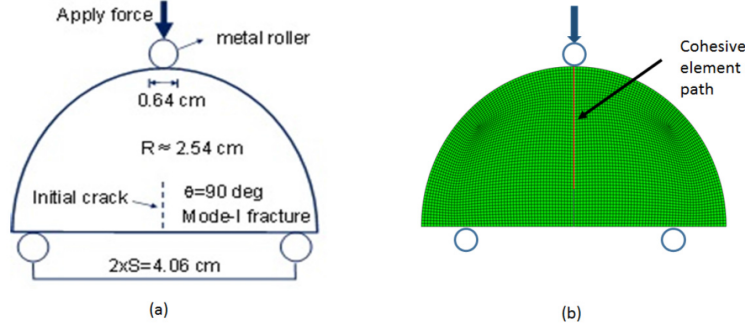


Figure 3.7: Semicircular Bending Test. a) Laboratory sketch, b) numerical mesh where the red line represents the cohesive elements

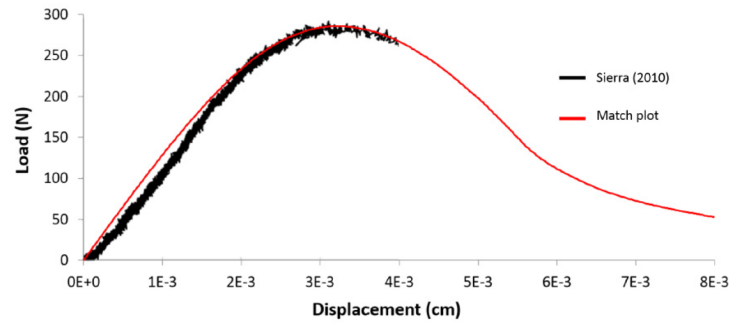


Figure 3.8: Match results of numerical simulation and lab experiments

where E' is the plane-strain modulus of elasticity ($E' = E/(1 - \nu^2)$)

The finite element simulation was used for the analysis using ABAQUS software. The reservoir was modeled with 4-node plane strain elements with a dimension of 50 x 50 meters. Both hydraulic fracture and natural fracture were modeled with 6-node cohesive elements, 4-nodes for displacement and two middle-pressure nodes. Both fractures were extended all along the length of the sketch. The reservoir and fractures were defined using sections. The assembly of the parts was made with tie constraint and contact interaction. The hydraulic fracture was represented by red horizontal elements in the sketch. Natural fracture intersects the hydraulic fracture perpendicularly at the middle of its length. The injection point was located five meters away from the intersection along the hydraulic fracture.

3.6 References

- Advani, S., Lee, T., and Lee, J., 1990, Three-dimensional modeling of hydraulic fractures in layered media: part I finite element formulations (in *Journal of Energy Resources Technology* 112 (1): 19.
- Atkinson, B. K., and Meredith, P. G., 1987, Experimental fracture mechanics data for rocks and minerals, *Fracture mechanics of rock*, 477525, ISBN: 978-0-12-066266-1 published by Elsevier.
- Akulich, A.V. and Zvyagin, A.V., 2008. Interaction between hydraulic and natural fractures. *Fluid dynamics*, 43(3), pp.428-435.
- Barenblatt, G., 1962, The mathematical theory of equilibrium cracks in brittle fracture (in *Advances in applied mechanics* 7 (1): 55-129.
- Batchelor, G. K., 1967, *An Introduction to Fluid Dynamics*. Cambridge University Press.
- Biot, M. A., 1941, General theory of three-dimensional consolidation (in *Journal of applied physics* 12 (2): 155-164.
- Bouchard, P., Bay, B., and Chastel, Y., 2000, Crack propagation modelling using an advanced remeshing technique (in *Computer methods in applied mechanics and engineering* 189 (3): 723-742.
- Bowker, K.A., 2007, Barnett shale gas production, Fort Worth Basin: Issues and discussion. *AAPG bulletin*, 91(4), pp.523-533.
- Carter, B., Wawrzynek, P.A. and Ingraffea, J., 2000, Automated 3-D crack growth simulation (in *International Journal for Numerical Methods in Engineering* 47 (1-3): 229-253.
- Chen, Zuorong, Bungler, A.P., Zhang, Xi, and Jeffrey, Robert G, 2009, Cohesive zone finite element-based modeling of hydraulic fractures (in *Acta Mechanica Sinica* 22 (5): 443-452.
- Chen, Z., 2012, Finite element modelling of viscosity-dominated hydraulic fractures (in *Journal of Petroleum Science and Engineering* 88: pp. 136-144.
- Cipolla, C.L., Warpinski, N.R., and Mayerhofer, M., 2008, *The Relationship Between Fracture Complexity Reservoir Properties and Fracture Treatment Design*, Society of Petroleum Engineers.
- Cleary, M.P. and Wong, S.K., 1985, Numerical simulation of unsteady fluid flow and propagation of a circular hydraulic fracture (in *International Journal for Numerical and Analytical Methods in Geomechanics* 9 (1): 114.
- Cleary, M.P., Wright, C.A. and Wright, T.B., 1991, Experimental and modeling evidence for major changes in hydraulic fracturing design and field procedures. In *SPE Gas Technology Symposium*. Society of Petroleum Engineers.

- Coussy, O., Dangla, P., Lassabatre, T., and Baroghel-Bouny, V., 2004, The equivalent pore pressure and the swelling and shrinkage of cement-based materials (in *Materials and structures* 37 (1): 15-20.
- Dahi Taleghani, A. and Lorenzo, J.M., 2011, An Alternative Interpretation of Microseismic Events during Hydraulic Fracturing. *Proc.*
- Dahi Taleghani, A. and Olson, J.E., 2011, Numerical modeling of multistranded-hydraulic-fracture propagation: Accounting for the interaction between induced and natural fractures (in *SPE Journal* 16 (03): 575-581.
- Dahi Taleghani, A. and Olson, J. E., 2013, How Natural Fractures Could Affect Hydraulic-Fracture Geometry (in *SPE Journal* (Preprint).
- Dahi-Taleghani, A., Puyang, P., Le Calvez, J. and Lorenzo, J., 2013, Post-Treatment Assessment of Induced Fracture Networks, SPE-166354-MS presented in SPE Annual Technical Conference and Exhibition in New Orleans, LA, USA.
- Daneshy, A.A., 1974, Principles of hydraulic fracturing. In *Proceedings of the Solution Mining Symposium*. New York: American Institute of Mining, Metallurgy, and Petroleum Engineers (pp. 15-32).
- Dugdale, D.S., 1960, Yielding of steel sheets containing slits (in *Journal of the Mechanics and Physics of Solids* 8 (2): 100-104.
- Jeffrey, R. G., Vandamme, L. , and Roegiers, J. C., 1987, Mechanical interactions in branched or subparallel hydraulic fractures. *Society of Petroleum Engineers*.
- Jeffrey, R.G., Zhang, X. and Thiercelin, M.J., 2009, Hydraulic Fracture Offsetting in Naturally Fractured Reservoirs: Quantifying a Long-Recognized Process, *Society of Petroleum Engineers*.
- Gale, J.L.W., Reed, R.M. and Holder, J., 2007, Natural fractures in the Barnett Shale and their importance for hydraulic fracture treatments (in *AAPG bulletin* 91 (4): 603-622.
- Hanson, M.E., Shaffer, R.J. and Anderson, G.D., 1981, Effects of various parameters on hydraulic fracturing geometry. *Society of Petroleum Engineers Journal*, 21(04), pp.435-443.
- Hennings, P.H., Olson, J.E. and Thompson, L.B., 2000, Combining outcrop data and three-dimensional structural models to characterize fractured reservoirs: An example from Wyoming. *AAPG bulletin*, 84(6), pp.830-849.
- Holditch, S.A., 2006, Tight gas sands (in *Journal of Petroleum Technology* 58 (6): 86-93.
- Hopkins, C. W., Rosen, R. L., and Hill, D. G., 1998, Characterization of an induced hydraulic fracture completion in a naturally fractured Antrim shale reservoir. *Society of Petroleum Engineers*.
- Iwashita, K and Oda, M., 2000, Micro-deformation mechanism of shear banding process based on modified distinct element method (in *Powder Technology* 109 (1): 192-205.

- Jarvie, D. M., Hill, R. J., Ruble, T. E., and Pollastro, R. M., 2007, Unconventional shale-gas systems: The Mississippian Barnett Shale of north central Texas as one model for thermogenic shale-gas assessment. AAPG bulletin, 91(4), 475-499.
- Lamont, N. and Jessen, F.W., 1963, The effects of existing fractures in rocks on the extension of hydraulic fractures. Journal of Petroleum Technology, 15(02), pp.203-209.
- Laubach, S. E., 2003, Practical approaches to identifying sealed and open fractures (in AAPG bulletin 87 (4): 561-579.
- Le Calvez, J. H., Tanner, K. V., Glenn, S. A., Kaufman, P. S., Sarver, D. R., Bennett, L. A., and Palacio, J. C., 2006, Using induced microseismicity to monitor hydraulic fracture treatment: a tool to improve completion techniques and reservoir management, SPE Eastern Regional Meeting, Society of Petroleum Engineers.
- Lorenz, J.C., and Sharon J.F., 1989, Differences in Fracture Characteristics and Related Production: Mesa verde Formation Northwestern Colorado. SPE formation, 4(01), 11-16.
- Martha, L.F., Wawrzynek, P.A, Ingraffea, A.R., 1993, Arbitrary crack representation using solid modeling (in Engineering with Computers 9 (2): 6382.
- Narr, W., Schechter, D. and Thompson, L., 2006, Naturally fractured reservoir characterization, Richardson, TX: Society of Petroleum Engineers (Reprint).
- Olson, J. E. and Dahi-Taleghani, A., 2009, Modeling simultaneous growth of multiple hydraulic fractures and their interaction with natural fractures. Proc.
- Ortega, O. J, A Marrett, R. and Laubach, S.E., 2006, A scale-independent approach to fracture intensity and average spacing measurement (in AAPG bulletin 90 (2): 193-208.
- Rogner, H.H., 1997, An assessment of world hydrocarbon resources. Annual review of energy and the environment, 22(1), pp.217-262.
- Sarris, E and Papanastasiou, P., 2011a, The influence of the cohesive process zone in hydraulic fracturing modelling (in International Journal of Fracture 167 (1): 3345.
- Sarris, E and Papanastasiou, P., 2011b, Modeling of hydraulic fracturing in a poroelastic cohesive formation (in International Journal of Geomechanics 12 (2): 160167.
- Shapiro, A.M, Andersson, J., 1983, Steady state fluid response in fractured rock: a boundary element solution for a coupled, discrete fracture continuum model (in Water Resources Research 19 (4): 959969.
- Seeburger, D.A. and Zoback, M.D., 1982, The distribution of natural fractures and joints at depth in crystalline rock (in Journal of Geophysical Research: Solid Earth (19782012) 87 (B7): 5517-5534.
- Sierra, R., Tran, M.H. and Abousleiman, Y.N., 2010, Woodford Shale mechanical properties and the impacts of lithofacies. 110.

- Valencia, K.J.L., Chen, Z. and Rahman, S.S., 2005, Design and Evaluation of Hydraulic Fracture Stimulation of Gas and Coal Bed Methane Reservoirs Under Complex Geology and Stress Conditions. In International Petroleum Technology Conference. International Petroleum Technology Conference.
- Wang, Y., Yin, X., Ke, F., Xia, M., and Peng, K., 2000, Numerical simulation of rock failure and earthquake process on mesoscopic scale (in pure and applied geophysics 157 (11-12): 1905-1928.
- Warpinski, N.R. and Teufel, L.W., 1987, Influence of geologic discontinuities on hydraulic fracture propagation (includes associated papers 17011 and 17074) (in Journal of Petroleum Technology 39 (02): 209220.
- Wilson, C.R and Witherspoon, P.A., 1974, Steady state flow in rigid networks of fractures (in Water Resources Research 10 (2): 328335.
- Zhang, X. and Jeffrey, R.G., 2008, Reinitiation or termination of fluid-driven fractures at frictional bedding interfaces (in Journal of Geophysical Research: Solid Earth (19782012) 113 (B8).

Chapter 4

Two-dimensional Hydraulic Fracturing Model*

4.1 Introduction

CZM has been explained in the previous chapter. Conceptually, fracture initiation can be defined by δ_0 or T_{max} and the fracture propagation by δ_f or G_c . The cohesive interface is introduced as a layer of elements with zero thickness to predict initiation and growth of a possible fracture. It is notable that due to the importance of fluid pressure in the development of the failure zone, a coupled fluid flow and deformation model have been incorporated in the cohesive elements. Moreover, the model is considered large enough to avoid any potential interference with boundaries. The fracture process zone (unbroken cohesive zone) is defined within the separating surfaces where the surface tractions are nonzero (Figure 4.1).

There are three failure mechanisms present during the opening of crack in the cohesive zone, i) fracture initiation criterion, which is referred to as the beginning of degradation due to the stresses and/or strains that satisfy damage initiation criteria, ii) fracture evolution, fracture propagation when the stress intensity factor at the tip exceeds the rock toughness, and iii) when the cohesive elements are completely damaged and beyond this point the cohesive element no longer exists. The cohesive element approach removes stress singularity

*Part of this chapter 4 previously appeared as "Gonzalez-Chavez, M. A., Dahi-Taleghani, A., and Olson, J. E., 2015, A Cohesive Model for Modeling Hydraulic Fractures in Naturally Fractured Formations. Society of Petroleum Engineers." and "Gonzalez-Chavez, M. A., Puyang, P., and Dahi-Taleghani, A., 2015, From Semi-Circular Bending Test to Microseismic Maps: An Integrated Modeling Approach to Incorporate Natural Fracture Effects on Hydraulic Fracturing. Society of Petroleum Engineers.". There are reprinted by permission of Society of Petroleum Engineers (Appendix A).

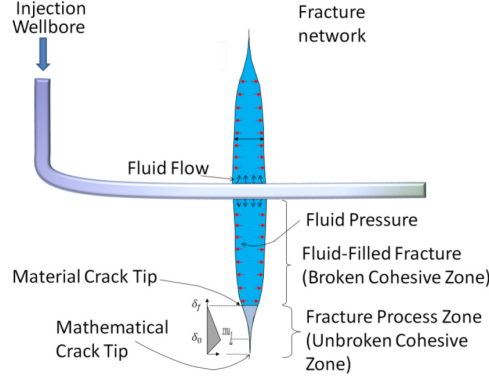


Figure 4.1: Cohesive elements at the tip of a hydraulic fracture are shown above. Two zones can be identified in a fracture: i) broken cohesive zone where traction-separation law is no longer valid, and ii) unbroken cohesive zone.

at the fracture tips, thereby improving the numerical stability of the model. Additionally, fracture models based on Griffith's criterion cannot really predict fracture initiation, which is made possible in the cohesive element approach.

Sarris and Papanastasiou (2011b) used cohesive elements to model the propagation of a plane strain single hydraulic fracture. By taking advantage of the problem symmetry, they reduced the problem to one-fourth. They considered poroelasticity for the cohesive elements and both poroelastic and elastic models for the matrix. Later, Chen (2012) extended this method for modeling penny-shaped hydraulic fractures using cohesive elements. They examined the influence of the opening fracture and injection pressure variation at critical separation at damage initiation (δ_0), cohesive strength (T_{max}), and the ratio of critical separation and failure damage (α). Chen's simulation considered the surrounding rock as an elastic medium and modeled the problem with axisymmetric geometry.

In this chapter, it is shown that fracture intersection can be modeled using CZM using the propose Semicircular Bending Test (SCBT) described in the previous chapter to determine cohesive properties of rock and cemented natural fractures. Parameter sensitivity studies provided in this chapter will help understand the role of different parameters to determine whether fracture crosses over the natural fracture or not.

4.2 Numerical Definition at the Intersection

Natural fractures and possible paths for the growth of the hydraulic fracture are defined with cohesive elements. Cohesive elements used here are linear quadrilateral coupled poroelastic elements. Each element consists of two pressure nodes (yellow dots for approach hydraulic fracture and green dots for intersected natural fracture) and four displacement nodes (red dots). Swept orientation for these cohesive elements is defined in the fracture opening direction. Pressure nodes are located at the middle of the element side in the direction of fracture propagation. At all the intersection points, path orientation is assumed to be the same as the approach hydraulic fracture (Figure 4.2,a). To assure the fluid flow continuity at the intersection, left pressure node of the element associated with approaching fracture and bottom pressure node of the intersected fracture is linked, and right pressure node of the cohesive element of the approaching crack is linked with the upper pressure node of the element corresponding to the intersected fracture (Figure 4.2,b).

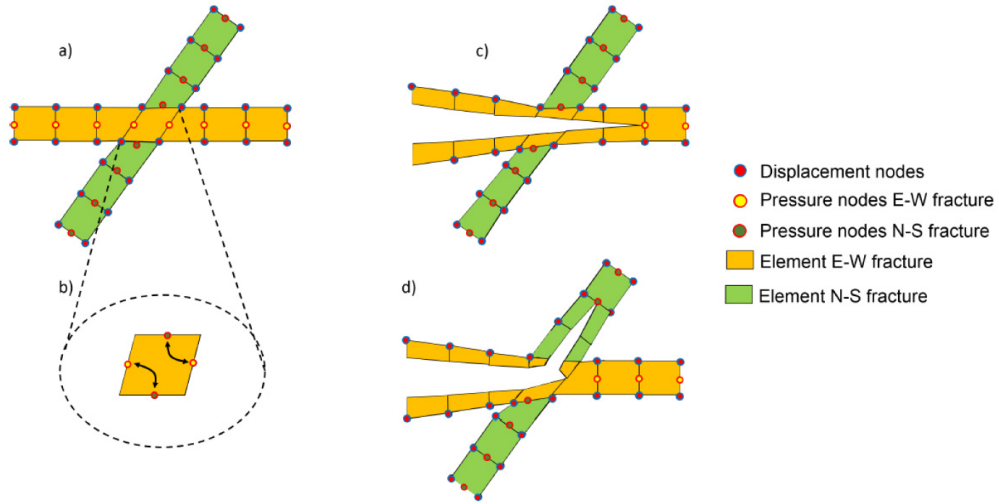


Figure 4.2: Sketch of cohesive elements arrangement at the intersection of a growing hydraulic fracture and a pre-existing natural fracture: a) before propagation reaching the intersection point, b) zoom-in of coupling of pressure nodes at the intersection, c) case when fracture crosses over the natural fracture, and d) diversion of the hydraulic fracture into natural fracture

Then, the direction of fracture propagation at the intersection is determined as it provides a larger relative energy release rate, which is determined not only by local differential stresses but also by the cohesive properties of rock and natural fractures. Figure 4.2,c and 4.2,d show different scenarios that may occur at the intersection like fracture crossover or diversion into the natural fracture, respectively.

Continuation of fracture propagation inside the natural fracture after diversion also depends on the relative energy rate ratio between propagation through the intact rock or through the natural fracture (Dahi-Taleghani, 2010).

Keeping δ_0 and δ_f for both rock and natural fracture constant, then the ratio of the fracture energy of rock and natural fracture will remain equal to the ratio of the maximum tensile strength of rock and cemented natural fracture as shown in Equation 4.1.

$$Factor = \frac{[G_c]_{NF}}{[G_c]_{HF}} = \frac{[T_{max}]_{NF}}{[T_{max}]_{HF}} = \frac{[K_n]_{NF}}{[K_n]_{HF}} \quad (4.1)$$

Values of Factor 0.2 and 3, based on values of Table 3.1, were considered in the simulations (Figure 4.3).

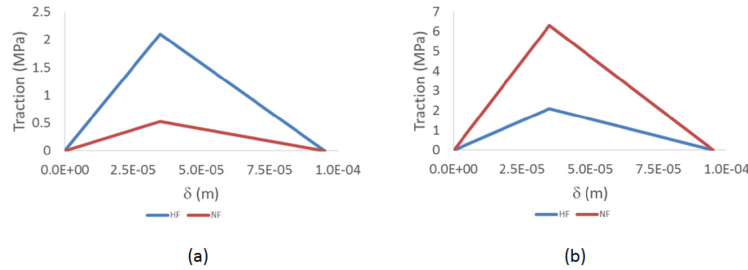


Figure 4.3: Cohesive properties of the formation rock and cemented natural fractures. a) rock with weaker cohesive properties, b) rock with stronger cohesive properties in comparison to the cemented natural fractures

4.3 Validation of CZM: Hydraulic Fracturing Opening in Presence of Natural Fracture

Blanton (1982) provided an equation that shows if the opening of the hydraulic fracture will be crossed, diverted or arrested once it reaches a natural fracture (Equation 4.2). If angle vs. differential horizontal stress field are plotted for a constant fracture energy, a line curve as shown in figure 4.4 is obtained. The hydraulic fracture opening will be diverted through natural fracture for any point below this curve. On the other side, the hydraulic fracture will cross the natural fracture at any point above this curve. Blanton also pointed out that a point close to this line will result in arresting of the opening of the hydraulic fracture.

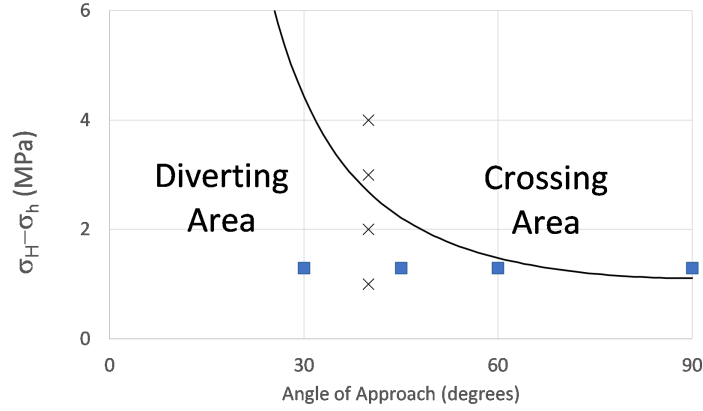


Figure 4.4: Plot to define whether the opening of the hydraulic fracture will be diverted, crossing or arrested once it reaches a natural fracture based on differential horizontal stress and angle (Blanton, 1982).

$$\sigma_H - \sigma_h = \frac{\sqrt{\frac{\pi E G_n}{4(1 - \nu^2)L}}}{\sin(\theta)^2} \quad (4.2)$$

where L is the distance from the injection point to the intersection, and θ is the angle between the fractures.

Eight different cases were considered to verify the solution: four cases for constant angle and different horizontal stress field (1, 2, 3, and 4 MPa cross points in figure 4.4), and four cases for constant horizontal stress field and four different angles (30, 45, 60, and 90 degrees' blue squares points in figure 4.4). Figure 4.5 shows the opening of hydraulic fracture and natural fracture (left and right plot in figure 4.5 respectively). It can be seen that the hydraulic fracture opening is diverted through the natural fracture for case 1 and 2 MPa and that the opening crosses the natural fracture for case 3, and 4 MPa which is expected based on results of figure 4.4 (blue square points).

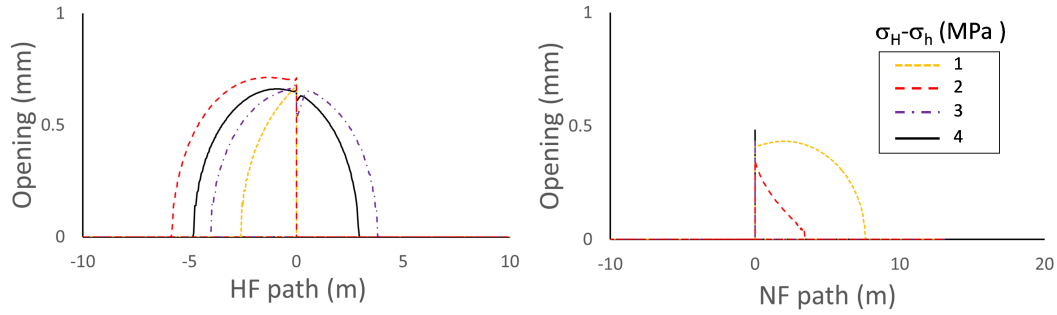


Figure 4.5: Opening when natural fracture path intersects hydraulic fracture with differential horizontal stress field of 1, 2, 3, and 4 MPa. The left picture shows the opening of the hydraulic fracture and the right picture shows the opening of the natural fracture. X-axis at zero mts shows the intersection between the fractures.

In the simulations carried out, the natural fracture path intersects the hydraulic fracture path at 30, 45, 60, and 90 degrees. Results in figure 4.6 show that opening of the natural fracture reduces as the angle of intersection increases. It can be seen that all cases show the opening of the hydraulic fracture diverts through natural fracture path except for a 90-degrees case, which crosses the natural fracture. These observations explain the sharp changes in the fracture path that create bottlenecks in fractures, which can cause challenges in proppant transport regardless of rock or fracturing fluid properties. The industry is very familiar with the concept of near wellbore and tip screenout. Based on these simulations, it is possible to conclude that screenouts may occur due to the intersection of natural fractures unless fine proppants like mesh 100 or mesh 120 are used for propping fractures.

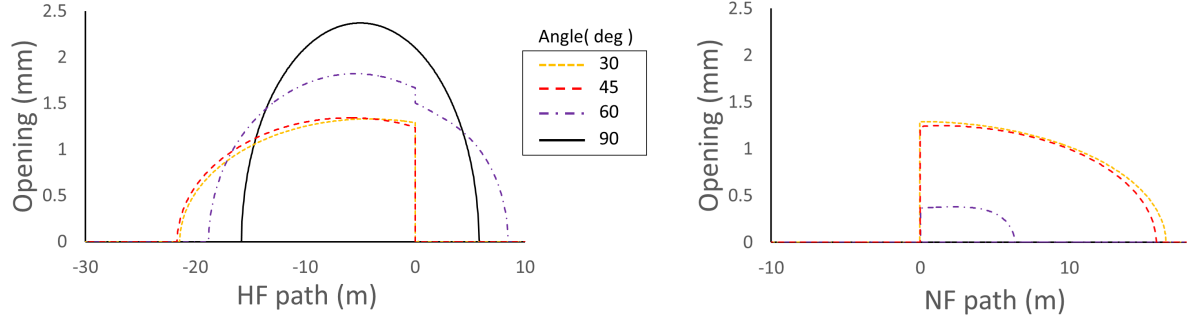


Figure 4.6: Opening when natural fracture path intersects hydraulic fracture at 30, 45, 60, and 90 degrees. The left picture shows opening of hydraulic fracture, and the right picture shows opening of natural fracture. X-axis at zero meters shows the intersection between the fractures.

4.4 Results

Figure 4.7 shows finite element meshes built for modeling interaction between hydraulic fracture and natural fractures. In Figure 4.7,a, both fractures are perpendicular to each other (like Barnett Shale) while in Figure 4.7,b, they are at a 45 degrees angle with each other. Table 3.1 summarizes the properties of the bulk rock and cohesive parameters used in case A and B. The injection point is located at the hydraulic fracture path and 1.00 meter away the intersection with the natural fracture.

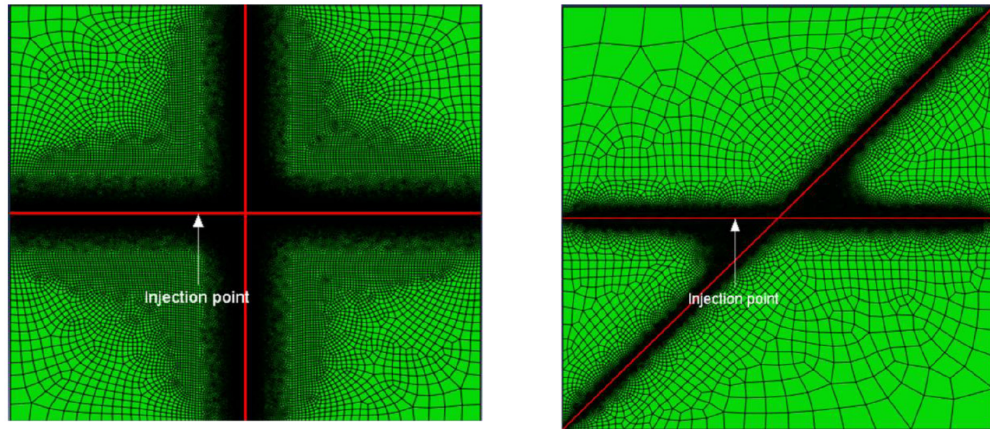


Figure 4.7: Sketch of the model in Abaqus software to simulate the intersection of a hydraulic fracture (horizontal red line) and a natural fracture (vertical red line) for 90 degrees (Left figure) and 45 degrees (Right figure).

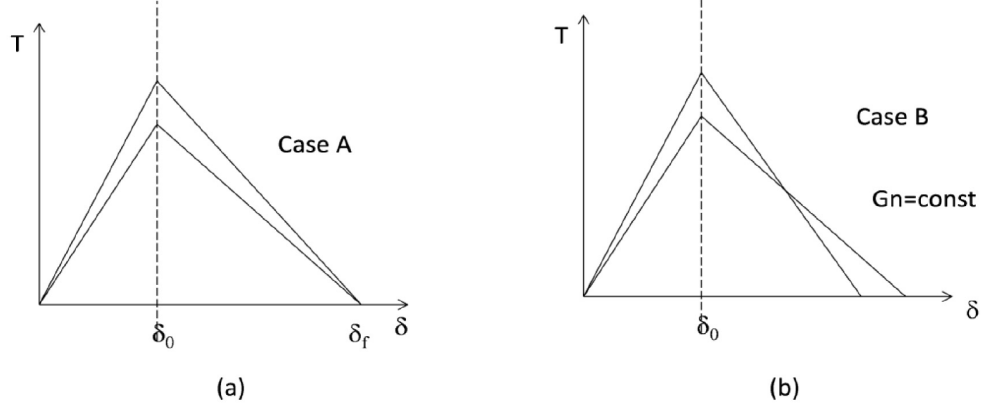


Figure 4.8: Cohesive properties of hydraulic fracture and natural fracture for case A and B.

Two parameter sensitivity studies are implemented here to show the effect of different cohesive parameters on the interaction between a growing hydraulic fracture and intersected natural fracture: The first parameter to be tested is the tensile strength of cement inside natural fracture T_{max} (Case A) while keeping ductility of the rock constant i.e. (δ_f , and δ_0), obviously a change of the cement strength will change the fracture toughness proportionally (see Figure 4.8,a). In the previous works of Dahi Taleghani and Olson (2011), only fracture toughness of the rock is considered to determine whether hydraulic fracture diverts into the natural fracture or crosses over. As an example, quartz can be represented as a natural cement with high strength and calcite as a one with low strength. In the second case (Case B), the toughness of the rock is kept constant while ductility of the rock is changed by changing the critical final opening δ_f Figure 4.8,b shows how cohesive parameters are changing in this case.

The cases analyzed in this chapter are summarized in Table 4.1

4.4.1 Case A. Effect of the Natural Cement Strength

In the first case, a hydraulic fracture intersects the natural fracture at a right angle with a tensile strength that is 20 percent of the value of the tensile strength of the intact rock (Figure 4.8,a). It can be seen that the fracture propagates until it reaches the intersection with the natural crack; then, the hydraulic fracture increases in width without further growth

Table 4.1: Cases analyzed for two-dimensional model

A	Natural Strength
B	Cement Ductility
C	Non-Perpendicular Fracture Intersection
D	Natural fracture with weak bonding (Factor=0.2)
E	Natural fracture with strong cement bonds (Factor=1)
F	Weak cement bonds in the natural fracture (Factor=0.2)
G	Natural fractures with strong cement bonds (Factor=1)
H	MultiNatural fractures with weak bonding (Factor=0.2)

in the matrix. Therefore, pumping more fluid leads to a wider rather than a longer fracture (Figure 4.9,a). In the case of limited proppant entry into the natural fracture system, this situation can be interpreted like a screenout as the liquid phase of the fracturing fluid drains into the natural fracture system and the fracturing fluid starts dehydrating inside the hydraulic fracture. However, the hydraulic fracture continues its propagation along the natural fracture; a choke is observed along the fracture inside natural crack (See the deflection point in Figure 4.9,b) which is in agreement without other numerical results for intersections (Dahi-Taleghani and Olson, 2011). The pressure of the hydraulic fracture propagates until reaching the intersection and beyond this point the hydraulic fracture is only ballooning without further growth (Figure 4.9,c). Even in the case of very high fracture toughness (tensile strength) in the natural fracture, CZM always predicts some limited reactivation along natural fractures. The pressure drop along the natural fracture was not considerable (Figure 4.9,d).

In the second case, the behavior of hydraulic fracture is tested when the natural fracture has tensile strength 10 times bigger than tensile strength of the hydraulic fracture (Figure 4.8,a). Figure 4.10,a shows that the opening of the hydraulic fracture is normal until reaching the intersection with the natural fracture. After this point, the hydraulic fracture is arrested at the intersection but continues its propagation in the other wing side, i.e., asymmetric fracture propagation similar to scenarios earlier discussed by Zhang and Jeffrey (2008). Figure 4.10,b shows how the pressure regularly develops until reaching the intersection with the

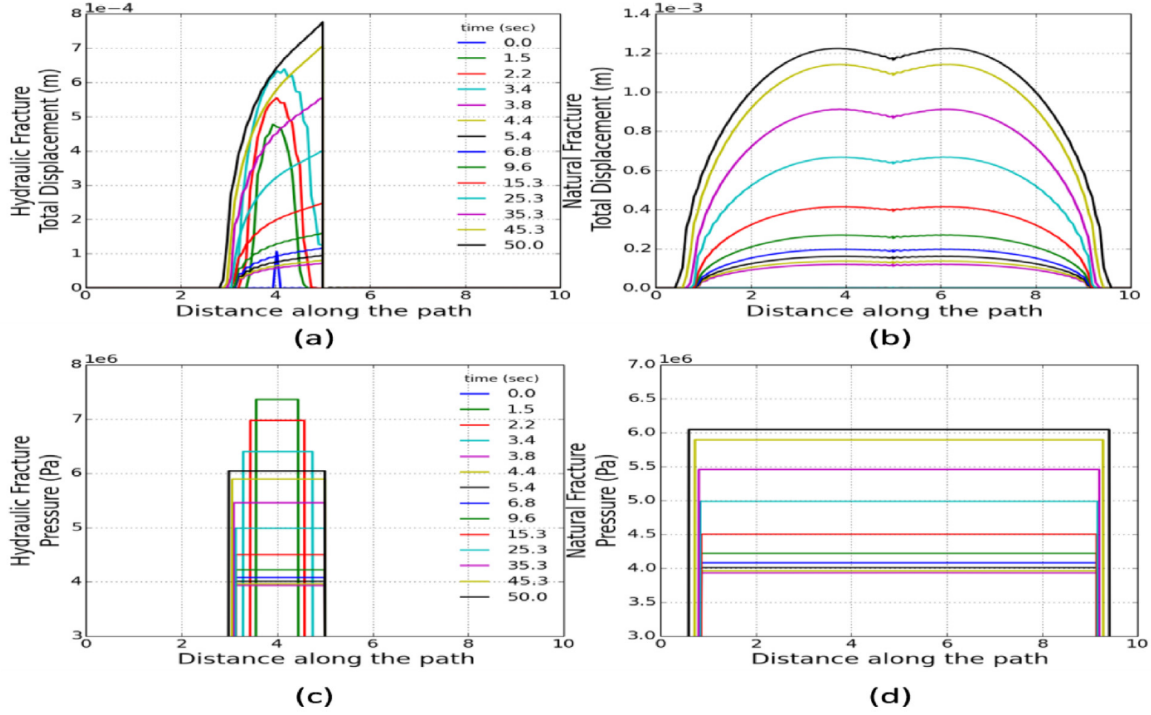


Figure 4.9: Perpendicular model, case A with factor 0.2, (a) hydraulic fracture opening, (b) natural fracture opening, (c) pressure propagation along hydraulic fracture path, and (d) pressure propagation along natural fracture path

natural fracture. Beyond this point, the fracture propagates only in the left-hand side till this fracture builds-up enough pressure to divert back into the matrix on the right side.

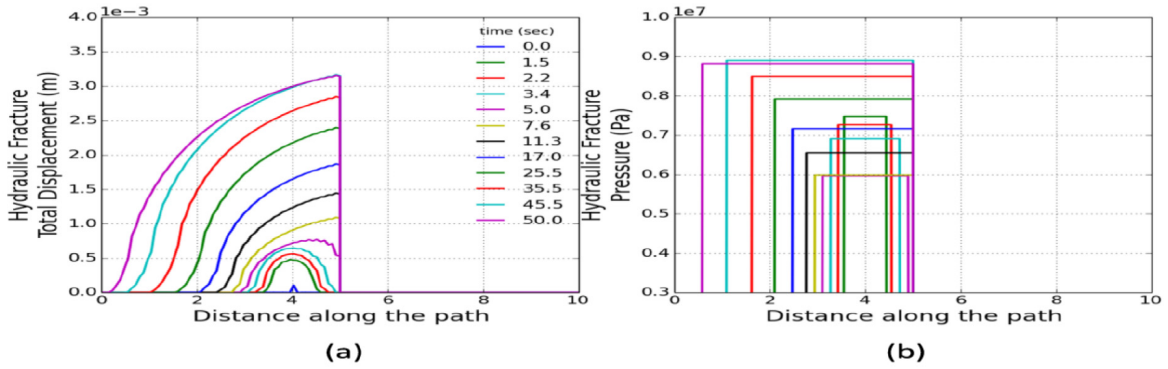


Figure 4.10: Perpendicular model, case A with factor 10, (a) hydraulic fracture opening. (b) Pressure profile along hydraulic fracture path

4.4.2 Case B. Natural Cement Ductility

In case B, behavior of hydraulic fracture, which is perpendicular to intersecting natural fracture with 20 percent lower failure opening (δ_f) while tensile strength is increased to keep the fracture toughness constant (Figure 4.8,b). Hydraulic fracture and natural fracture show similar opening and pressure behavior that were observed in case A (Figure 4.11). On the other side, different behavior is observed for the hydraulic fracture when the tensile strength is 5 times bigger than the value of the tensile strength of the hydraulic fracture with lower failure opening (δ_f), compared to the corresponding failure opening of the hydraulic fracture (Figure 4.8,b). It can be seen in Figure 4.12,a that the hydraulic fracture crosses the natural fracture, but the fracture opening is slower in the right-hand side than in the left-hand side of the hydraulic fracture. The opening of the natural fracture is not observed, but the geometry of the hydraulic fracture is affected by the presence of the natural fracture.

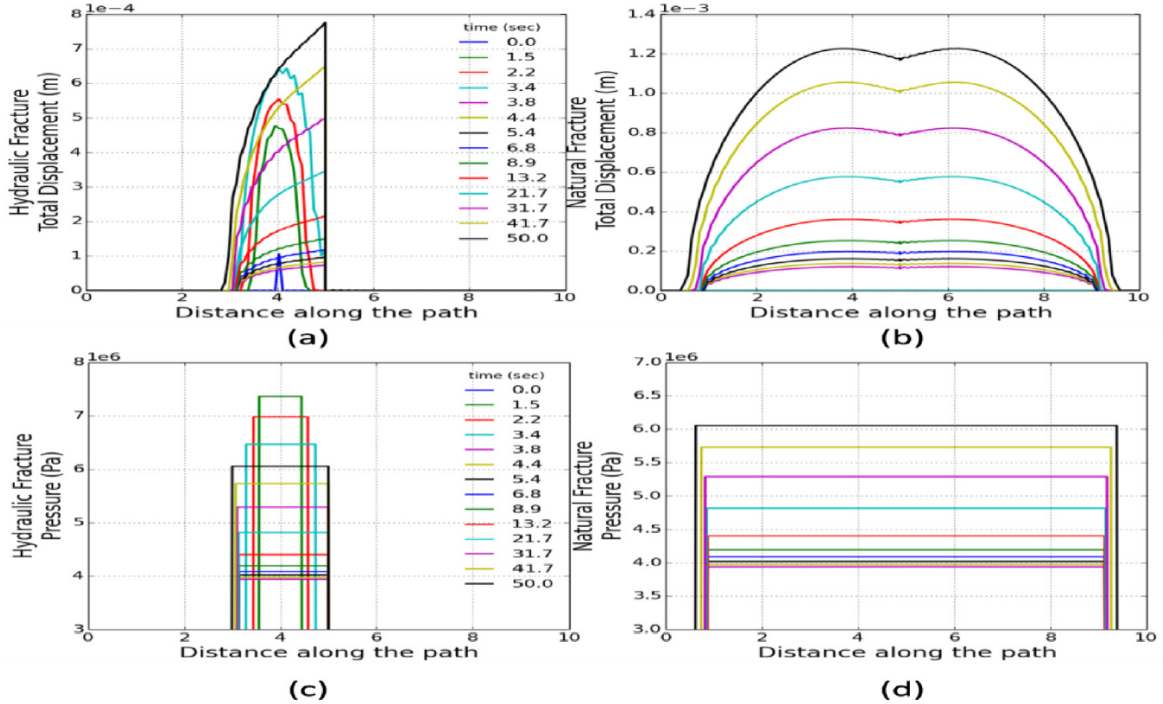


Figure 4.11: Perpendicular model, case B with factor 0.2, (a) hydraulic fracture opening, (b) natural fracture opening, (c) pressure propagation along hydraulic fracture path, (d) pressure propagation along natural fracture path.

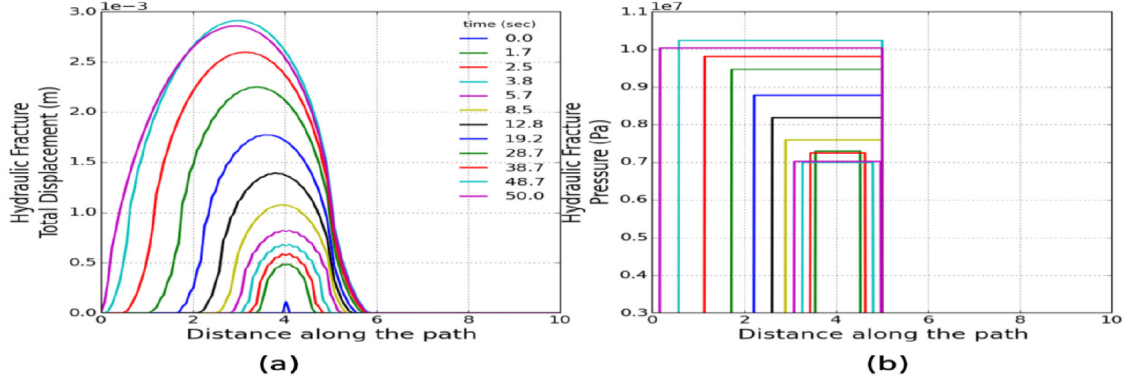


Figure 4.12: Perpendicular model, case A with factor 0.2, (a) Hydraulic fracture opening, (b) pressure propagation along natural fracture path

4.4.3 Case C. Non-Perpendicular Fracture Intersection

Natural fractures usually are not perpendicular to the direction of current maximum horizontal stress. Therefore, it is considered a non-perpendicular (45 degrees) intersection for previous cases A and B (Figure 4.8,a) and factors of 0.2, 1, and 2 for cement tensile strength. It can be seen for all cases that opening of hydraulic fracturing is deflected by the presence of a natural fracture, and the fracture only propagates along the preferred side of the natural fracture, while the main fracture gets wider (ballooning). Considering the height constraint in three-dimensional geometries, ballooning is not a stable process and leads to resumption of fracture growth in the main branch (Figure 4.13,b).

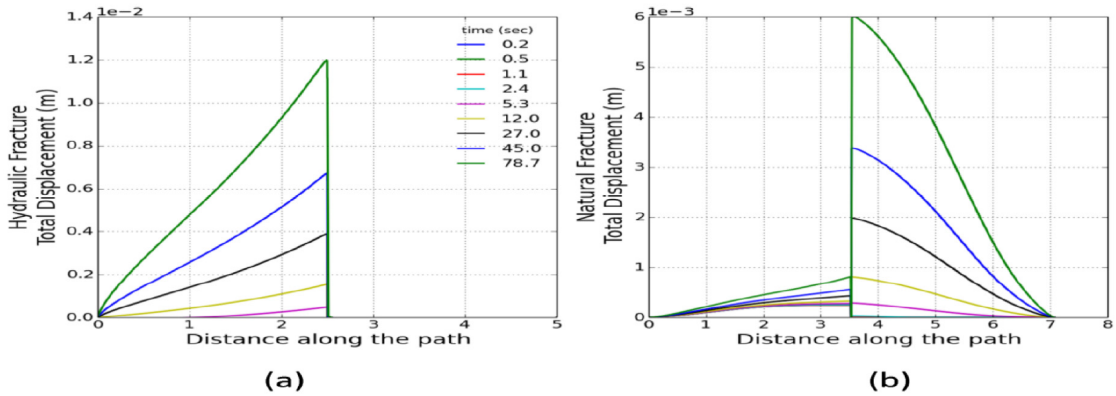


Figure 4.13: Opening (left) and pressure (right) propagates only in the left side of the hydraulic fracture.

The investigation in this chapter was limited to two-dimensional methods here. The key simplification is that the plane strain model assumes that the fracture is infinite in extent in one direction. This is not necessarily a good assumption, but the presented model is a preliminary model testing an entirely new method, and for computational simplicity, it was chosen to sacrifice the three-dimensional aspects of the problem. A more reliable model must ultimately add those three-dimensional aspects back in the calculation. Hence, the three-dimensional analysis is required to solve this problem in the general case for multilayered geological systems. The main obstacle to extending this tool to three-dimensional analysis is the computational time. The finite element mesh at the intersection of the fractures should be defined in such a way that fracture behavior at the intersection point would be dependent on local stresses and cohesive parameters rather than the mesh configuration. The models presented here assumed no hydraulic communication with natural fractures before being opened by the hydraulic fracture. In other words, natural fractures are assumed to be occluded with diagenetic materials. Cases for interaction with single and multiple natural fractures are presented to show the robustness of this approach.

4.4.4 Case D: Natural fracture with weak bonding (Factor=0.2)

Figure 4.14,a and ,b show opening of the hydraulic fracture along its original path and along the natural fracture, respectively. It can be seen how the opening of the hydraulic fracture is expanding normally until the fracture tip reaches the intersection with the natural fracture. Beyond this point, hydraulic fracture opening is reduced in width due the fact that the natural fracture takes most of the pumped fluid, hereafter. The right-side opening of the hydraulic fracture seems to become wider than the opening at the injection point due to this change in fluid movement. The opening in the left-side of the hydraulic fracture continues propagating but at a lower speed than before the hydraulic fracture reached the intersection with a natural fracture.

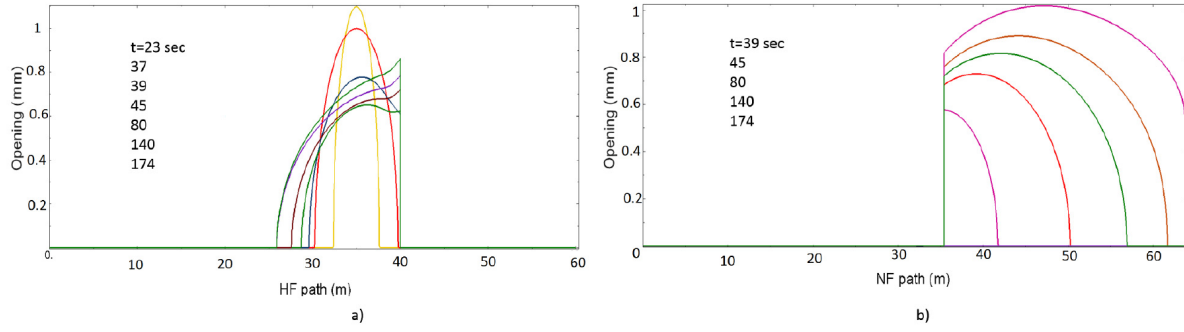


Figure 4.14: The opening profile for Factor=0.2. a) Opening of the hydraulic fracture with intersection point at 40 m. away from the wellbore. b) Opening along the natural fracture

Figure 4.15,a shows pressure front propagation along the original path of the hydraulic fracture. It can be seen how the pressure profile has the same pressure all along the open fracture at that time. With time, the following profiles have lower pressures for larger fracture lengths. Right-side pressure propagation is arrested once the hydraulic fracture profile reaches the intersection with the natural fracture. Figure 4.15,b shows pressure front propagation in the natural fracture in the wing with a larger angle with the original direction of the hydraulic fracture. Pressure declination in the natural fracture with time is lower than pressure declination of hydraulic fracture due to propagation along natural fracture requiring higher energy to keep propagating in the new direction.

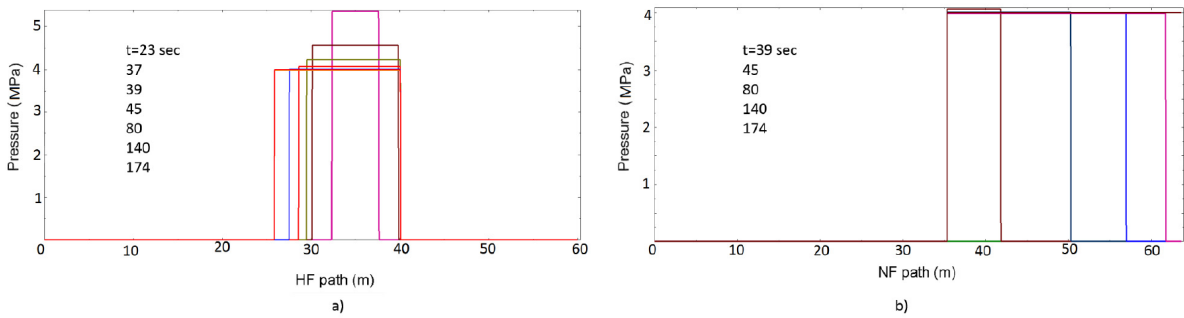


Figure 11—Pressure profile for Factor=0.2. a) hydraulic fracture and b) natural fracture

Figure 4.15: Pressure profile for Factor=0.2. a) hydraulic fracture and b) natural fracture

4.4.5 Case E: Natural fractures with strong cement bonds (Factor=1)

Figure 4.16,a shows total opening of hydraulic fracture at different times. It can be seen that the opening is normal in both wings of the hydraulic fracture. The presence of natural fracture does not affect the propagation of hydraulic fracture essentially because the opening of natural fractures did not occur.

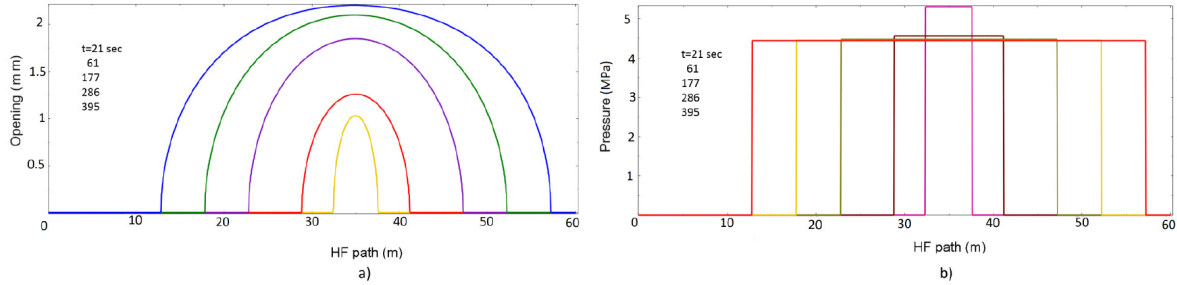


Figure 4.16: a) The opening profile of hydraulic fracture for Factor=1.0. Presence of natural fracture did not affect the opening in the hydraulic fracture. b) Pressure profile of hydraulic fracture

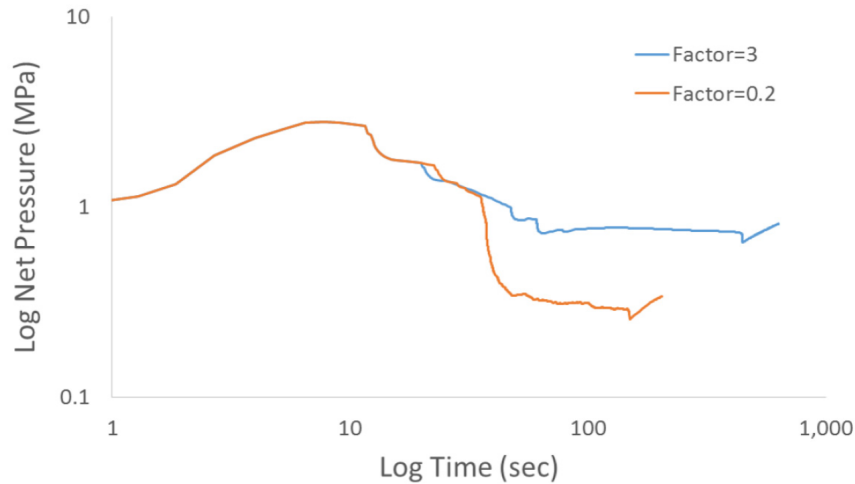


Figure 4.17: Bottomhole net pressure is compared when the hydraulic fracture crosses the fracture and when the path is diverted through natural fracture path

Figure 4.16,b shows the pressure profiles of hydraulic fracture at different times. It can be seen that pressure front propagation is also normal and symmetric on both wings. Figure 4.17 shows the net pressure profile for the case of weak natural fracture i.e. Factor=0.2 (red

line) and strong natural fracture i.e. Factor=1 (blue line). For Factor 0.2, it can be seen that pressure is increasing until the breakdown point is reached. Subsequently, the pressure declines slowly until hydraulic fracture tip reaches the intersection with the natural fracture. Net pressure after that time shows a larger pressure drop than when the hydraulic fracture was propagating. In addition, it can be seen that after that pressure drop, net pressure seems to remain almost constant due to the pressure necessary to let the natural fracture propagates. For Factor=1, a similar net pressure behavior can be seen at the beginning. Beyond this point, net pressure remains almost constant as the hydraulic fracture propagates, as hydraulic fracture needs less energy to continue propagating once it crosses the natural fractures. The last segment of net pressure starts to increase due boundary effects. According to Nolte and Smith (1981), positive slope corresponds to propagation in length, mode III. It can be seen how for Factor=1 that the slope is slightly higher than zero, which agrees with the Nolte-Smith pressure analysis theory. Nevertheless, for Factor=0.2, the negative slope, mode IV, rather corresponds to an increase in fracture length, corresponding to the opening that has diverted through the natural fracture. It can be seen as a slightly negative slope during hydraulic fracture propagation along the natural fracture.

Figure 4.18,a shows the bottomhole net pressure response for three different differential stresses (when maximum horizontal stress is equal, 5 and 10 percent higher than the minimum horizontal stress, respectively) for Factor 0.2 and 1. It can be seen for factor 0.2 that the lower net pressure drop corresponds to isotropic stress conditions, which look similar to Factor 1 case until natural fracture creates the net pressure drop in the last part. For anisotropic tectonic stress conditions, it can be seen that net pressure drop occurs at earlier times because propagation is faster and the negative slope corresponds to mode IV. Therefore, it means that propagation is not along the original hydraulic fracture path but in a different direction.

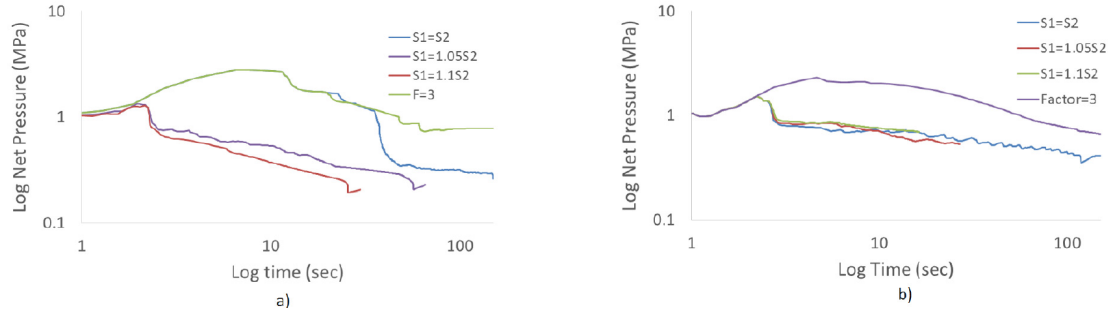


Figure 4.18: Net pressure comparison for different stress fields for sketch: a) 45 degrees and b) 90 degrees for different stress fields

In cases 3 and 4, a situation is considered where natural fractures are aligned in the direction parallel to current minimum horizontal stress. Hence, hydraulic fractures are approaching natural fractures at 90 degrees. Barnett shale is a good example of this situation.

4.4.6 Case F: Weak cement bonds in the natural fracture (Factor=0.2)

Figure 4.19,a and ,b show the opening hydraulic fracture and a portion of the hydraulic fracture that is diverted into the natural fracture at different times, respectively. It can be seen how hydraulic fracture propagation on the other end is slowed down as most of the pumped fluid is moving to open the natural fracture toward one of its wings; although, after a while, the other wing of natural fracture may open up. This phenomenon can be explained by the high lower energy that is required to open natural fracture in comparison to the intact rock. The magnitude of the opening in the hydraulic fracture and its comparison with the opening of the natural fracture confirms this situation. Additionally, the net pressure was obtained from the same three stress fields (Figure 4.18b). Net pressure drop occurs almost at the same time for Factor 0.2 case, and declination looks linear in the log-log plot.

4.4.7 Case G: Natural fractures with strong cement bonds (Factor=1)

Similar behavior is observed like results shown in Figure 4.16,a and ,b. Hydraulic fracture propagation is propagated as the natural fracture does not exist. This is expected when hydraulic fracture propagates regardless of the angle of the natural fracture when the prop-

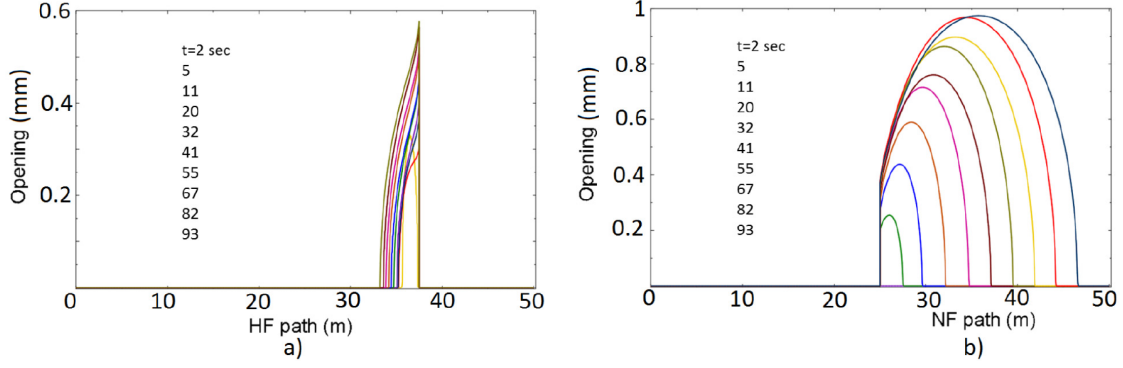


Figure 4.19: Opening profile for the case with Factor=0.2. a) Opening along the original path of the hydraulic fracture. b) The opening of the part of hydraulic fracture expanded along the natural fracture

erties of the natural fracture are greater than the properties of the hydraulic fracture. The difference in stress field (Figure 4.18,b) also did not affect net pressure, which is always higher than what it is in the Factor 0.2 case.

4.4.8 Interaction with multiple natural fractures

Similar to the case with a single natural fracture, simulations are carried out for a hydraulic fracture executed in a formation with more than one set of natural fractures or a grid of natural fractures at a 90 degrees angle with respect to each other as shown in Figure 4.20. Natural fracture distribution in Marcellus shale is very similar to this configuration. The initial hydraulic fracture path is represented by one east-west fracture at the center of the sketch. Natural fractures are represented by four east-west and four north-south fractures, which are equally spaced. It is considered two different geometries: 1) fractures have equal spacing of 5 meters for a model with dimensions of 100 x 100 meters, and 2) fractures with 24m spacing (Figure 4.20). The wellbore in these models is located in the middle of the middle east-west fracture in the center.

The injection is assumed to lead to laminar flow, the possible tortuosity because of the complex nonplanar geometry and turbulence due to high injection rates is neglected. Lubrication equation is assumed to be sufficient to describe fluid flow inside the fracture

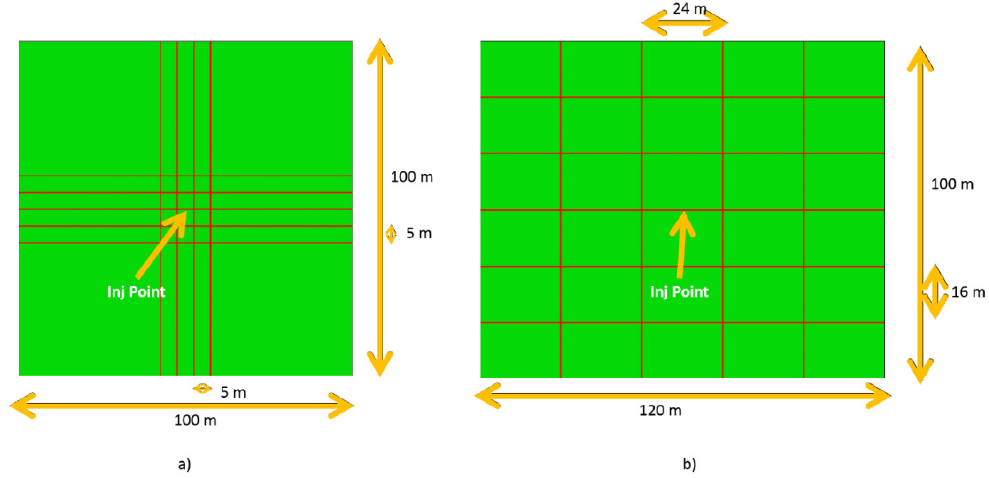


Figure 4.20: Computational models built to simulate the propagation of a hydraulic fracture in a network of natural fractures are shown above. a) sketch with a spacing of 5 meters between fractures, and b) spacing of 24 meters in the horizontal direction and 16 meters in the vertical direction. The wellbore in both sketches is shown by a black dot in the center

network. The reservoir rock is modeled with 4-node plane strain elastic elements. Fractures are modeled with 6-node cohesive elements. Due to large stress concentration around fracture tips, a fine mesh is used close to the fractures to assure the accuracy of the solution and coarse mesh was used in the borders to reduce the computational cost. The mesh grid in both sketches is not included in the below figure to avoid losing the visualization of fracture paths.

Case H: Natural fracture with weak bonding (Factor=0.2)

Due to the weak bonding of natural fractures, the hydraulic fracture is diverted into the intersected fractures. Now, hydraulic fracture no longer propagates perpendicular to the direction of the minimum horizontal stress. Beyond this point, fracture propagation mainly occurs along natural fracture paths. In contrast to the case for single natural fracture (Figure 4.18,b) in which the net pressure was declining, for this case, net pressure increases as propagating fracture strands squeeze each other.

Figure 4.21,a shows for Factor=0.2 case that net pressure increases until it reaches break-down. Subsequently, the pressure declines slowly as the hydraulic fracture propagates. Then

a second pressure drop occurs when hydraulic fracture tip reaches the intersection with the natural fracture. The difference in stress field would not affect the net pressure drop when the natural fracture is felt. Lower net pressure drop is observed as anisotropy stress field increases.

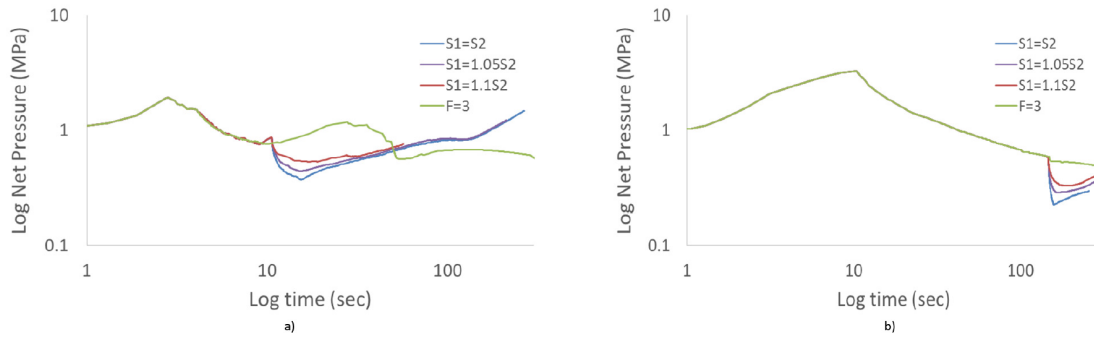


Figure 4.21: Net pressure behavior for a) sketch with 5 meters spacing among fractures, and b) higher spacing among the fractures

4.5 References

- Atkinson, B. K., and Meredith, P. G., 1987, Experimental Fracture Mechanics Data for Rocks and Minerals, Fracture Mechanics of Rock, 477525, ISBN: 978-0-12-066266-1 published by Elsevier.
- Baig, A.M., and Prince, M., 2010, Microseismic Moment Tensors: A Path to Understanding Growth of Hydraulic Fractures, paper SPE 137771 presented at the Canadian Unconventional Resources and International Petroleum Conference, Calgary, Canada.
- Barenblatt, G., 1962, The mathematical theory of equilibrium cracks in brittle fracture (in Advances in applied mechanics 7 (1): 55129.
- Blanton, T. L., 1982, An experimental study of interaction between hydraulically induced and pre-existing fractures. Society of Petroleum Engineers.
- Bedayat, H., and Dahi-Taleghani, A., 2014, Interacting Double Poroelastic Inclusions, Mechanics of Materials 69 (1), 204212.
- Cipolla, C.L., Warpinski, N.R., and Mayerhofer, M., 2008, The Relationship between Fracture Complexity Reservoir Properties and Fracture Treatment Design, Society of Petroleum Engineers.

- Dahi Taleghani, A. and J. Olson, 2009, Analysis of Multi-Stranded Hydraulic Fracture Propagation: An Improved Model for the Interaction Between Induced and Natural Fractures, SPE 124884, Presented in SPE hydraulic Fracturing Technology Conference in Woodland, TX.
- Dahi Taleghani, A., 2010, Fracture Re-Initiation as a Possible Branching Mechanism during Hydraulic Fracturing, ARMA 10-278, Presented in American Rock Mechanics in Salt Lake City, UT.
- Dahi Taleghani, A. and Olson, J.E., 2011, Numerical Modeling of Multistranded-Hydraulic-Fracture Propagation: Accounting for the Interaction between Induced and Natural Fractures (in SPE Journal 16 (03): 575581.
- Dahi Taleghani, A., Puyang, P., Le Calvez, J. and Lorenzo, J., 2013, Post-Treatment Assessment of Induced Fracture Networks, SPE-166354-MS presented in SPE Annual Technical Conference and Exhibition in New Orleans, LA, USA.
- Dahi Taleghani, A., Ahmadi, A., and Olson, J. E., 2013, Secondary Fractures and Their Potential Impacts on Hydraulic Fractures Efficiency, ISRM International Conference for Effective and Sustainable Hydraulic Fracturing. International Society for Rock Mechanics.
- Delaney, P. T., and Pollard, D. D., 1981, Deformation of host rocks and flow of magma during growth of minette dikes and breccia-bearing intrusions near Ship Rock, New Mexico (No. 1202). USGPO.
- Dugdale, D.S., 1960, Yielding of steel sheets containing slits (in Journal of the Mechanics and Physics of Solids 8 (2): 100104.
- Elices, M., Guinea, G. V., Gomez, J., and Planas, J., 2002, The Cohesive Zone Model: Advantages, Limitations and Challenges. Engineering fracture mechanics, 69 (2), 137163.
- Fan, L., Luo, F., Lindsay, G. J., Thompson, J. W., and Robinson, J. R., 2011, The bottom-line of horizontal well production decline in the Barnett Shale. In SPE Production and Operations Symposium. Society of Petroleum Engineers.
- Gale, J.L.W., Reed, R.M. and Holder, J., 2007, Natural Fractures in the Barnett Shale and Their Importance for Hydraulic Fracture Treatments (in AAPG bulletin 91 (4): 603622.
- Gonzalez, M., Dahi Taleghani, A. and Olson, J., 2015, A Cohesive Model for Modeling Hydraulic Fracturing in Naturally Fractured Formations, SPE 173384-MS, SPE Hydraulic Fracturing Technology Conference, 3-5 February, The Woodlands, TX, USA, doi: 10.2118/173384-MS.
- Gonzalez-Chavez, M. A., Puyang, P., and Dahi-Taleghani, A., 2015, From Semi-Circular Bending Test to Microseismic Maps: An Integrated Modeling Approach to Incorporate Natural Fracture Effects on Hydraulic Fracturing. Society of Petroleum Engineers.
- Holditch, S.A., 2006, Tight Gas Sands (in Journal of Petroleum Technology 58 (6): 8693.

- Hopkins, C. W., Frantz, J. H., Hill, D. G., and Zamora, F., 1995, Estimating Fracture Geometry in the Naturally Fractured Antrim Shale. Society of Petroleum Engineers. doi: 10.2118/30483-MS.
- Hopkins, C. W., Rosen, R. L., and Hill, D. G., 1998, Characterization of an induced hydraulic fracture completion in a naturally fractured Antrim shale reservoir. In SPE Eastern regional meeting (pp. 177186).
- Jeffrey, R.G., Zhang, X. and Thiercelin, M.J., 2009, Hydraulic Fracture Offsetting in Naturally Fractured Reservoirs: Quantifying a Long-Recognized Process, Society of Petroleum Engineers.
- Kresse, O., Weng, X., Gu, H., and Wu, R., 2013, Numerical modeling of hydraulic fractures interaction in complex naturally fractured formations. Rock mechanics and rock engineering, 46 (3), 555568.
- Laubach, S. E., 2003, Practical approaches to identifying sealed and open fractures: AAPG Bulletin, v. 87, p. 561579, doi: 10.1306 /11060201106.
- Maxwell, S. C., Urbancic, T. I., Steinsberger, N., Energy, D., and Zinno, R., 2002, Microseismic Imaging of Hydraulic Fracture Complexity in the Barnett Shale. SPE 77440.
- Murphy, H. D., and Fehler, M. C., 1986, Hydraulic fracturing of jointed formations (No. LA-UR-85-3701; CONF- 860325-1). Los Alamos National Lab., NM (USA).
- Nolte, K.G. and Smith, M.G., 1981, Interpretation of Fracturing Pressures. JPT 33 (9): 17971775. SPE-8297-PA.
- Ortega, O. J, A Marrett, R. and Laubach. S.E., 2006, A Scale-Independent Approach to Fracture Intensity and Average Spacing Measurement (in AAPG bulletin 90 (2): 193208.
- Patel, P. S., Robart, C. J., Ruegamer, M., and Yang, A., 2014, Analysis of US Hydraulic Fracturing Fluid System and Proppant Trends. Society of Petroleum Engineers. doi: 10.2118/168645-MS.
- Pollard, D. D., Muller, O. H., and Dockstader, D. R., 1975, The form and growth of fingered sheet intrusions. Geological Society of America Bulletin, 86 (3), 351363.
- Pommer, L., 2013, Using Structural Diagenesis to Infer the Timing of Natural Fractures in the Marcellus Shale (in URTEC).
- Potluri, N.K., 2005, The Effect of Natural Fractures on Hydraulic Fracture Propagation (in SPE European Formation Damage Conference).
- Puyang, P., B. Sarker and A. Dahi Taleghani, 2015, Multi-Disciplinary Data Integration for Inverse Hydraulic Fracturing Analysis: A Case Study presentation at the Unconventional Resources Technology Conference held in San Antonio, Texas, USA, 20-22 July 2015.
- Sato, T., Murota, M., and Shimizu, Y., 1998, Characteristics of Rayleigh and Leaky Surface Acoustic Wave Propagating on a La₃Ga₅SiO₁₄ Substrate. Japanese journal of applied physics, 37 (5S), 2914.

- Sierra, R., Tran, M.H. and Abousleiman, Y.N., 2010, Woodford Shale mechanical properties and the impacts of lithofacies. 110.
- Valencia, K. J. L., Chen, Z., Hodge, M. O., and Rahman, S. S., 2005, Optimizing stimulation of coalbed methane reservoir using multi-stage hydraulic fracturing treatment and integrated fracture modeling. In SPE Asia Pacific Oil and Gas Conference and Exhibition. Society of Petroleum Engineers.
- Warpinski, N.R. and Teufel, L.W., 1987, Influence of Geologic Discontinuities on Hydraulic Fracture Propagation (includes associated papers 17011 and 17074) (in Journal of Petroleum Technology 39 (02): 209220.
- Zhang, X. and Jeffrey, R.G., 2008, Reinitiation or Termination of FluidDriven Fractures at Frictional Bedding Interfaces (in Journal of Geophysical Research: Solid Earth (19782012) 113 (B8).

Chapter 5

Three-dimensional Hydraulic Fracturing Model

5.1 Introduction

Hydraulic fracturing is recognized as a solution for wellbores that cannot produce by itself after perforations due to the very low permeability of the reservoir rock. The treatment consists of pumping viscous fluid at high rates increasing the pressure at the formation until the rock breaks, and the fluid continues flowing through the expanding fracture. In a homogeneous isotropic formation, double wing symmetric fracture is expected to form in the subsurface (see Figure 5.1, a), however, Geometry and propagation of the hydraulic fracture may change due to the presence of natural fractures (Figure 5.1, b) to form a non-planar fracture.

Natural fractures (with length of meters) surrounding the wellbore may affect the direction of the hydraulic fracture propagation. These natural fractures might not be detected by conventional tools such as well logs, cores samples, and seismic due logs ratio of investigation is just few feet, cores samples are of small size, and seismic resolution can detect discontinuities higher than 30 meters. Figure 5.2 shows an example of Mexican oil field which consist of Upper Paleocene-Lower Eocene alternating sandstone and shale bodies. It can be seen a wide variation in clay-shale content and not continuous laminar extension through the reservoir.

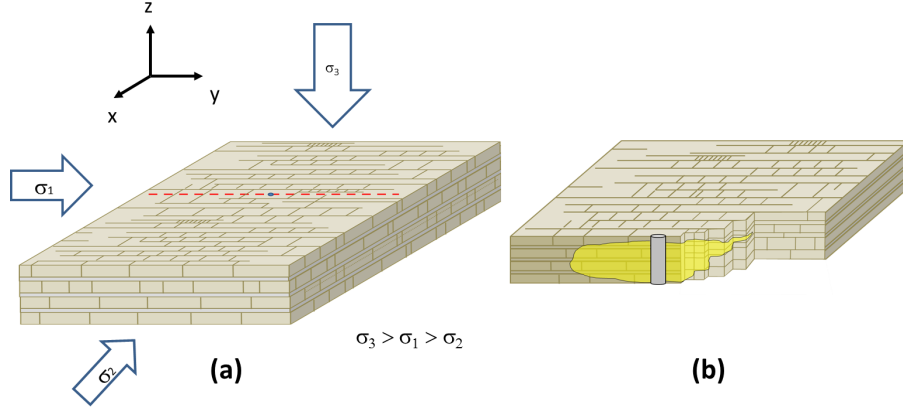


Figure 5.1: a) Schematic representation of a layered reservoir with natural fractures, where the ideal hydraulic fracture path (red dotted line) is expected to be perpendicular to the minimum horizontal stress (σ_2), b) probable hydraulic fracture geometry in the presence of natural fractures, which resembles the situation in the field.

Moreover, facies changes, which consist of sandstone and sand-rich alternating beds of sandstone (Abbaszadeh, 2003), promote rock properties changes through layering. At well-bore level, it can be seen in the gamma-ray log (left picture) that intercalation between sandstone and shales might be important in the pay zone. At seismic scale (right figure), discontinuity and pinch-outs make assuming uniform height fracture impossible, hence typical 2D models like PKN and KGD hydraulic fractures (Khristianovic and Zheltov, 1955, Perkins and Kern, 1961, Geertsma and De Klerk, 1969, Nordgren, 1972) even pseudo-3D models (Simonson *et. al*, 1978, Mack and Warpinski, 2000) cannot be fruitful to catch height varying geometry of these fractures even pseudo-3D models.

Different analytical and numerical models have been proposed for two- and three-dimensional geometries, however almost all of these models are limited to simplified geometries. In two-dimensions, Perkins and Kern (1961) and Nordgren (1972) formulated the famous PKN model, which represents the hydraulic fracture geometry better for fracture with larger fracture compared with its height. Khristianovic and Zheltov (1955) and Geertsma and De Klerk (1969) formulated the famous KDG model, which represent the hydraulic fracture geometry better for fracture with smaller fracture length than its height. These models do not consider vertical variations in layering. First approaches to three-dimensional models

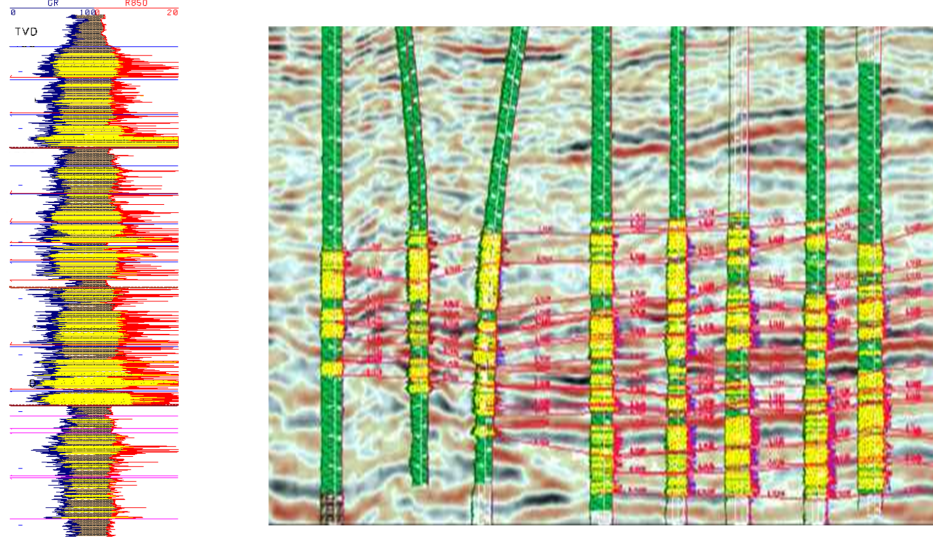


Figure 5.2: . Selection of the proper zone to perforate need to take in account interlayering of the rock at wellbore level and continuity of these layers through the reservoir. Left picture show gamma ray log intercalation of sandstone and shale. Right picture shows seismic and cross section of an unconventional reservoir basin with pinch-outs and discontinuities in Mexico.

were an extension of two-dimensional formulations. The first models were Pseudo-three-dimensional (P3D) (Simonson *et. al*, 1978) and planar 3D (PL3D) models (Clifton *et. al*, 1981). In P3D models; there are two types of approaches: cell-based and lumped models (Mack and Warpinski, 2000). In cell-based, the fracture length is sub-divided into a series of PKN-like cells. Lumped model divides the geometry of the fracture in two half-ellipses. Fracture length, the tip of the top and bottom ellipses are calculated every step time. In planar 3D models (PL3D), fluid flow equations and geometry of the fracture are described by a two-dimensional mesh of cells.

Linear Elastic Fracture Mechanics (LEFM) has been very successful in describing mechanics of fracture in brittle rocks. However, the success story has not repeated in the case of soft rocks (Atkinson and Meredith, 1987). LEFM neglects the details in the fracture process zone as it lumps all effects into the fracture tip stress singularity; however, a detailed description of the fracture process zone could be essential to understanding fracture behavior at the intersections or heterogeneous interfaces. In these situations, the size of the fracture

process zone is larger than the grain size, which violates the fundamental assumption of LEFM. Griffiths criterion states that fracture will propagate once fracture energy reaches the critical energy associated with the toughness of the rock (Griffith, 1921). However, this criterion is only limited to non-cohesive materials and can only predict the propagation of pre-existing fractures, not their initiation.

Cohesive Zone Method (CZM) has primarily evolved initially from the Dugdale-Barenblatt model (Dugdale, 1960, Barenblatt, 1962). In CZM, the fracture process is lumped into the fracture line and is characterized by a cohesive law that relates tractions and displacement jump across cohesive surfaces ($T - \delta$). Therefore, the rock behavior during fracturing is described by two constitutive laws: a linear stress-strain relationship for the bulk matrix and a cohesive surface relationship (cohesive law) that allows spontaneous prediction of fracture initiation and growth.

Hydraulic fracturing simulation in three-dimensional model has been extensively used in Linear Elastic Fracture Mechanics (LEFM) to solve different problems such as in-situ stress contrast between barriers and pay layers which is the major factor that controlled fracture height (Warpinski *et. al*, 1982, Teufel *et. al*, 1984), fracture toughness which fairly affect both fracture height and propagation (Thiercelin *et. al*, 1989), lower modulus of barrier zone may restrict the fracture height (Smith *et. al*, 2001, Gu *et. al*, 2006), shear strength of the interface between barrier zone and pay zone is small at shallow depths (Daneshy, 2009). However, few publications related to three-dimensional model using cohesive elements have been published. Zhang *et. al* (2010) used CZM in a three-dimensional model for hydraulic fracturing in horizontal wellbores in Daqing Oilfield, China. Zhang confirmed that in-situ stresses contrast has a higher impact on the hydraulic fracture geometry growth than others parameters such as modulus, tensile strength, and viscosity injection fluid. Wang *et. al* (2012) build multilayer 3D model for a horizontal wellbore to study the influence of in-situ stress field, elastic modulus, and tensile strength. They found that higher in-situ stress, lower elastic modulus, and higher tensile strength of barrier zones would promote

height reduced and fracture length enlarged. Wang *et. al* (2015) found that serious slippage between barrier and pay layer occurs, fracture tip becomes blunted, and fracture height is controlled when the shear strength of interface is lower than a critical value. No publications have been found at this moment related to the multi-fracture system using cohesive elements in a three-dimensional model.

The objective of this chapter is to develop a simulation tool based on CZM to predict and understand changes in the net pressure response in fracturing treatment to identify discontinuities and/or interlayer changes. The methodology described in this paper consists of the following steps: First, cohesive parameters are obtained by fitting load-displacement curve obtained from laboratory experiments with the numerical models. Those parameters were used as a benchmark (after upscaling) to simulate field-scale hydraulic fracturing problems. A special modification is proposed to present elements containing fracture intersection to assure fluid flow and displacement continuity. In the following sections, we briefly discuss fracture interactions and cohesive zone method theory. In the results and discussion section, we will discuss the main results obtained in this study and the sensitivity analysis for some of the main parameters.

5.2 Numerical Implementation

Natural fractures and possible paths for the growth of the hydraulic fracture in the formation are defined with cohesive elements. Cohesive elements used here are linear quadrilateral coupled poroelastic elements (Figure 5.3). Each element consists of two pressure nodes (yellow dots for the approaching hydraulic fracture and green dots for the intersected natural fracture) and four displacement nodes (red dots). Swept orientation for these cohesive elements is defined in the fracture opening direction. Pressure nodes are located in the middle of the element sides in the direction of fracture propagation. To assure the fluid flow continuity at the intersection, the left pressure node of the element associated with the approaching fracture and bottom pressure node of the intersected fracture are linked, and right pres-

sure node of the cohesive element of the approaching crack is linked with the upper-pressure node of the element corresponding to the intersected fracture. Then, the direction of fracture propagation at the intersection is determined as the direction that provides larger relative energy release rate, which is determined not only by local differential stresses but also by the cohesive properties of rock and natural fracture.

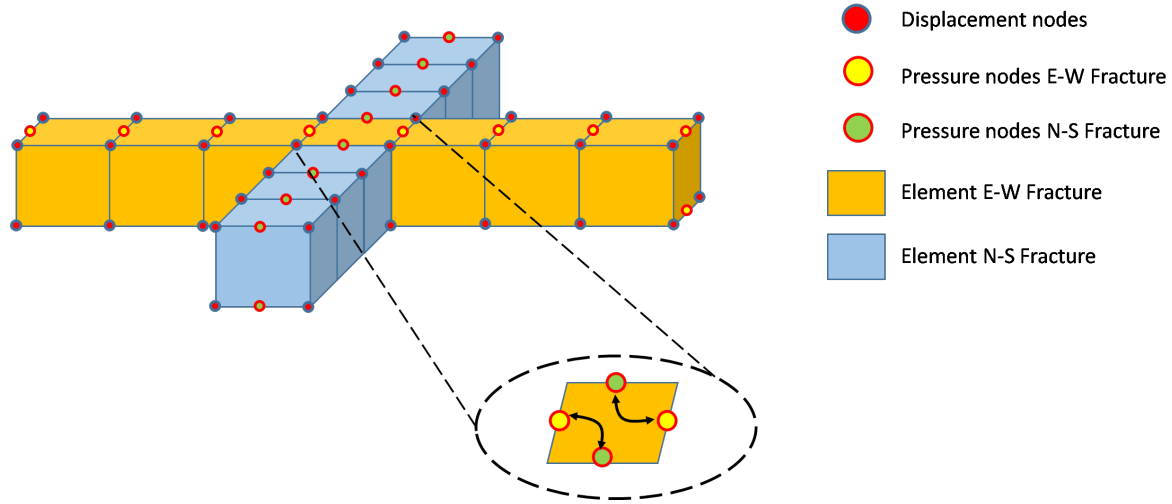


Figure 5.3: Sketch of cohesive elements arrangement at the intersection of a growing hydraulic fracture (orange path) and a pre-existing natural fracture (blue path). Zoom figure shows the share pressure nodes to assure the fluid flow continuity.

Cohesive parameters extracted from lab experiments based on the method described in the previous section are used, in this section, as benchmark values for running simulations in the field-scale. In this example, a natural fracture crosses the hydraulic fracture path at 30 degrees. The injection point is 10 meters away from the intersection between the fractures.

A three-dimensional finite element model is built to define the reservoir rock using 6-node linear triangular prism elements; the model dimensions are 100 m x 50 m x 5 m. A cohesive layer is inserted in the middle of the model to represent a possible path for fracture propagation using 12-node three-dimensional coupled cohesive elements consisted of 8 displacement nodes and 4 pore pressure nodes. Displacements at the boundaries of the model are constrained in the normal direction to impose height growth constraint out of the model. Figure 7 shows a sketch of the reservoir mesh with 294,000 elements and red

lines represent the cohesive elements for hydraulic and natural fracture paths with 3,727 elements. The nonlinear constitutive equation of the cohesive elements and their coupled nature increase the computational cost of simulations to limit them to smallest possible model with no boundary effect.

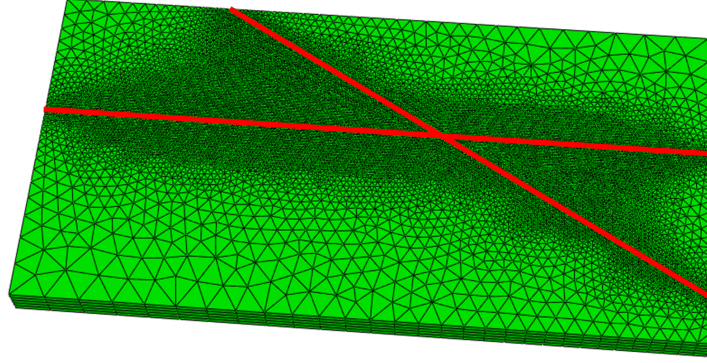


Figure 5.4: : Numerical sketch of the reservoir (green elements) and the path of the two cracks (red lines).

To better identify the configuration of the model demonstrated in Figure 5.4, Figure 5.5 shows the schematics of the formation rock in green, a possible hydraulic fracture path in orange, and the natural fracture in blue. The yellow zone on the left side of the hydraulic fracture path represent the zone where one or more layers will have different elastic properties (tougher or weaker) from the rest of the hydraulic path. That means that in both hydraulic and natural fractures, the layers cohesive properties might be different from the rest of the hydraulic fracture path. We will change the rock properties of these layers to understand how net pressure response will change. The beginning of the tougher/weaker zone is 5 meters away from the injection point and 15 meters away from the intersection of the fractures. Then, first the net pressure response of the tougher/weaker zone and later the effect of the intersection is expected to be seen.

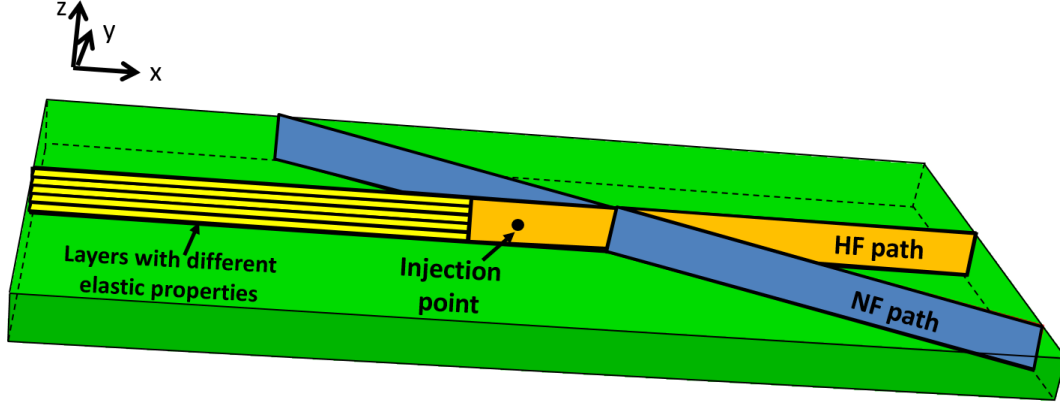


Figure 5.5: Schematic representation of three-dimensional model of one hydraulic fracture path (orange) that is intersected by a natural fracture at 30 degree (blue). Yellow zone represents lower or higher cohesive rock properties in the hydraulic fracture path (yellow). Injection point is 10 meters away of the intersection of the fractures and five meters away the beginning of the plug zone.

5.3 Validation of CZM: Hydraulic Fracturing 3D model

To validate the three-dimensional model, we use analytical solution from Dean and Schmidt (2009). It can be seen that numerical model using cohesive elements show similar opening with analytical solution (Figure 5.6).

$$x_f = \left\{ \frac{QEt}{\sqrt{\pi}(1-\nu^2)K_{IC}\Delta z} \right\}^{2/3} \quad (5.1)$$

where x_f is the half-fracture length, Q is the injection rate, E is Young's modulus, ν is Poisson's ratio, K_{IC} is the fracture toughness, and Δz is the height of the hydraulic fracture.

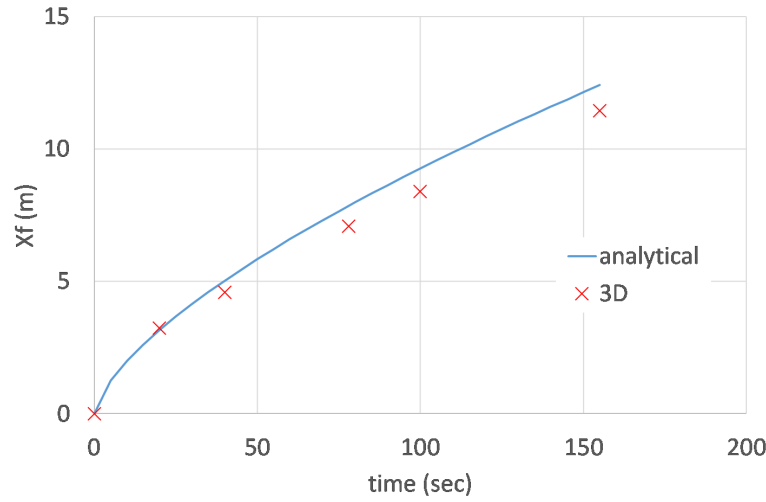


Figure 5.6: Comparison of half fracture length shows that analytical solution (Equation 5.1) gives higher fracture length than numerical model using cohesive elements.

5.4 Results and Discussion

Net pressure response was analyzed when the hydraulic fracture had different cohesive properties through its path. A zone with different rock properties (tougher/weaker) than the rest of the layer is defined (yellow color) in Figure 5.5 which is 5 meters away from the injection point and 15 meters away from the intersection. In this way, the response of the net pressure of the tougher/weaker zone earlier than the response of the intersection is expected to be seen. The opening of the fracture will be diverted through the natural fracture path when the cohesive critical energy is lower ($1/5$) in the direction of the natural fracture than in the direction of the hydraulic fracture. Blue line in Figure 5.7 shows net pressure is increasing like in conventional analysis of Nolte-Smith pressure interpretation (Nolte and Smith, 1981) because the hydraulic fracture is growing in a vertical direction up to reach the upper and lower boundaries at 23 seconds. Beyond this point, net pressure declines up to 160 seconds where is the time that net pressure reaches the intersection. An additional pressure drop is observed beyond this point because the propagation has changed the direction; now, through the natural fracture path.

The cases analyzed in this chapter are summarized in Table 5.1

Table 5.1: Cases analyzed for three-dimensional model

A	Plug in the middle hydraulic fracture path
B	Plug in the 2- and 4-layer of hydraulic fracture path
C	Plug in the 4- and 5-layer of hydraulic fracture path

In the first case, the tougher/weaker zone is located in the middle layer (Figure 5.7). We tested two scenarios: weak middle layer, where the critical energy of the yellow zone is 1/5 (red line) smaller than the rest of the layer; and tough middle layer, where the critical energy is five times (green line) larger than the rest of the layer. The red line shows an additional net pressure drop at 81 seconds because the effect of the weak weaker zone. It can be seen that the rest of the net pressure response follows the pattern of the first case with the difference that is a shift around 7 MPa.

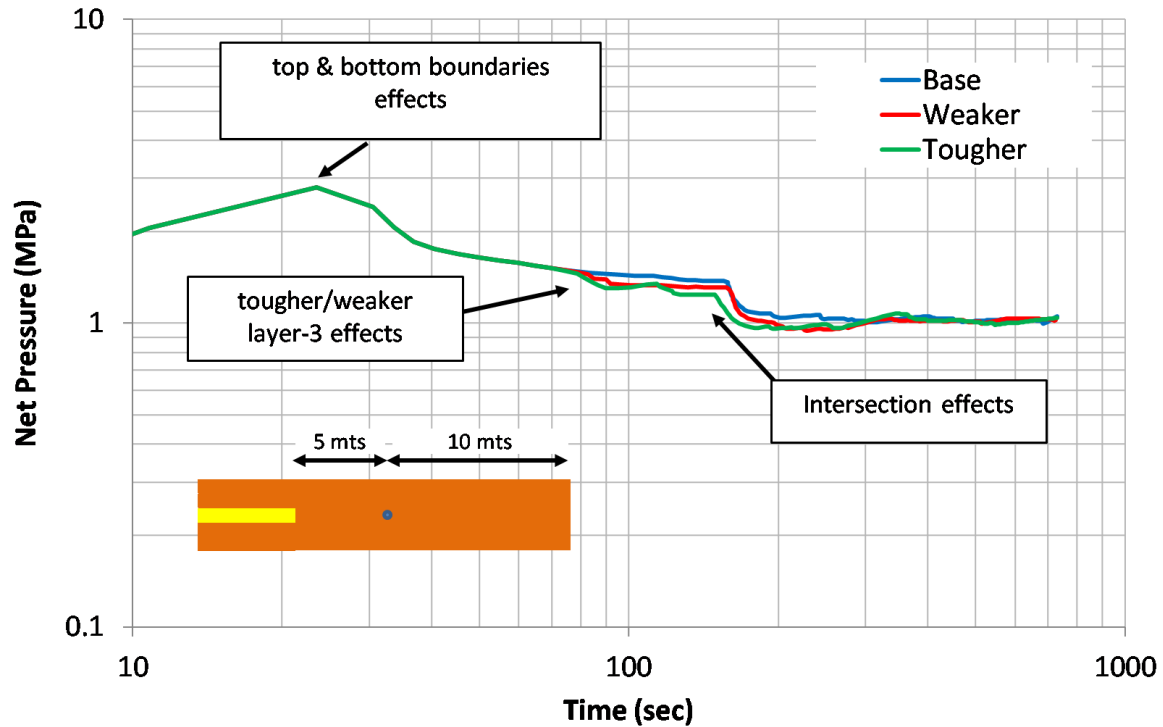


Figure 5.7: Net pressure response for the hydraulic fracture diverting into natural fractures: 1) when weaker layer case is in the natural fracture, and 2) when tougher layer case is in the middle layer of hydraulic fracture path.

On the other hand, for the tough zone scenario (green line), we still have the net pressure drop at 81 seconds, but now the intersection is at the shorter time because the hydraulic fracture is propagating faster in the direction of the intersection. Both cases continue the net response of the base case example (blue line) at around 300 seconds because yellow zone effects no longer affect net pressure response. Figure 5.8 shows contours plot for opening for both scenarios. It can be noticed that there are no big changes in both openings and net pressure drop.

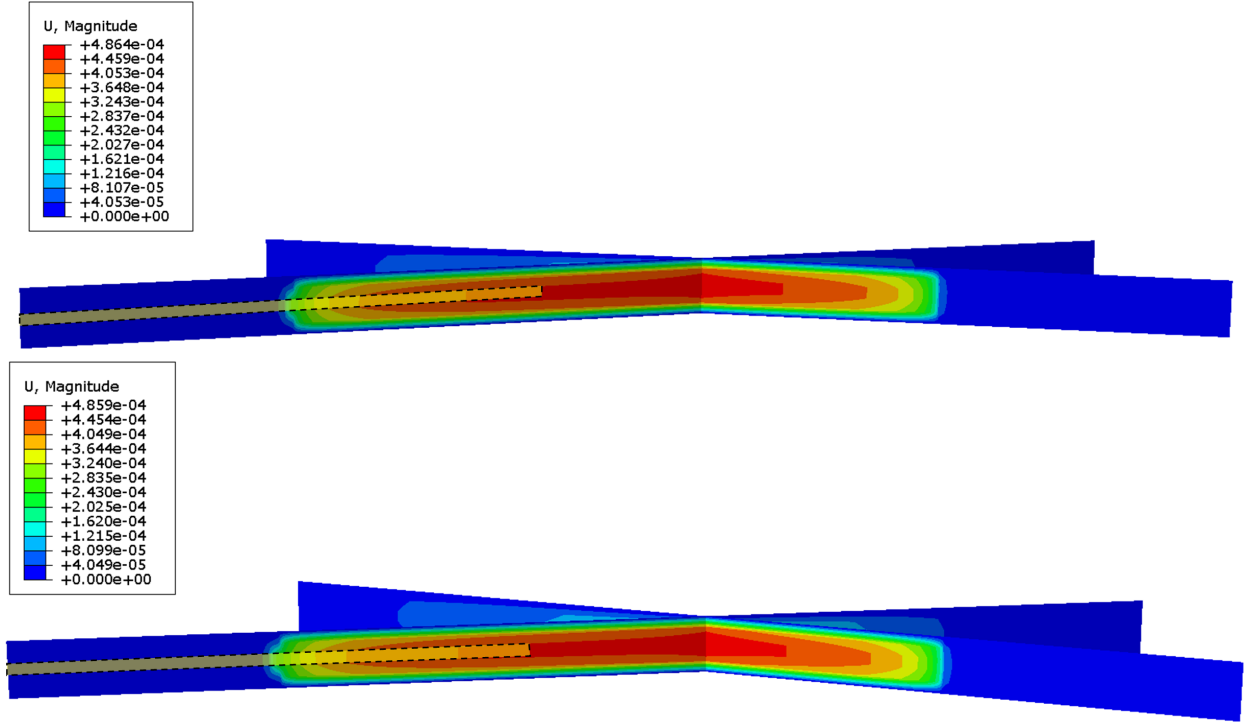


Figure 5.8: Case 1. Opening of hydraulic and natural fracture due presences of weak (upper figure) and tougher (bottom figure) layer on the middle layer of hydraulic fracture path.

In a second case, the tougher/weaker zone is in the second and fourth layers (yellow layers in Figure 5.9)). In this case, weaker yellow zone effects are felt earlier (at around 75 seconds). Weaker zones (red line) show higher net pressure drop than tougher yellow zone (green line) because weak layers make hydraulic fracture propagate faster (Figure 5.10) upper). Tougher zone show lower net pressure drop because now hydraulic fracture is propagating asymmetrically in the other direction of the tougher zone (Figure 5.10) bottom).

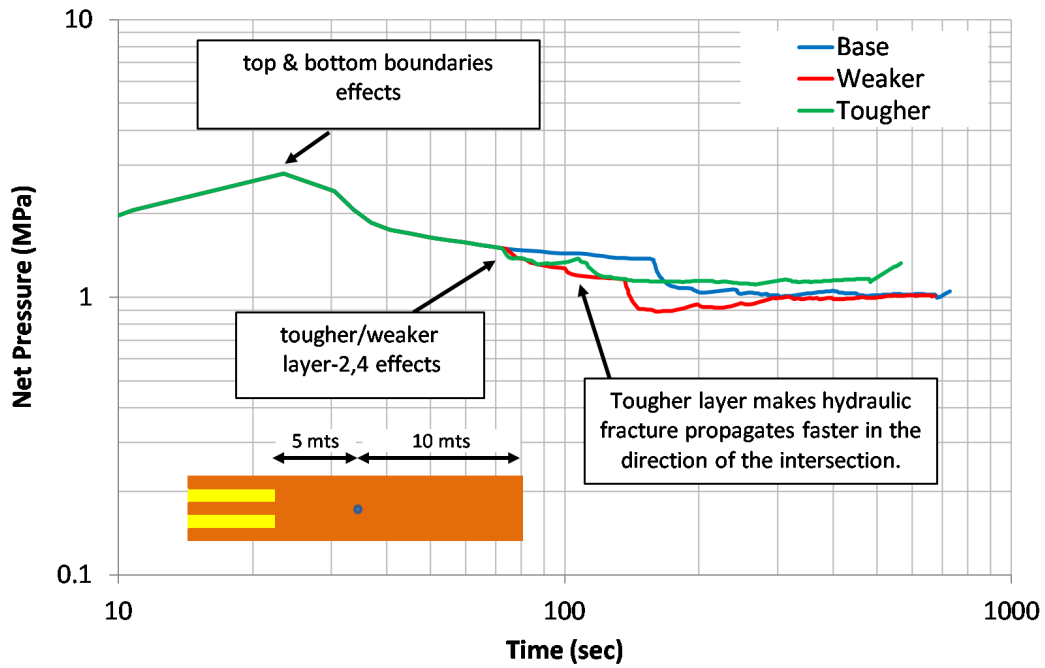


Figure 5.9: Case 2. Net pressure response when Tougher/weaker layer is in the middle layer. Weaker layer case shows extra net pressure drop and Tougher layer case shows faster propagation in the other direction.

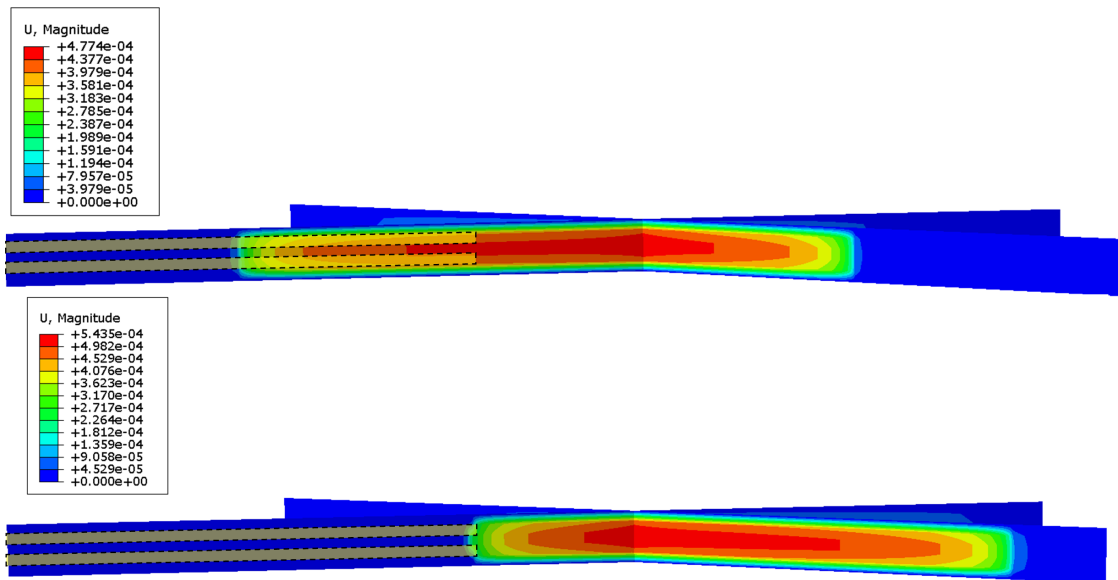


Figure 5.10: Case 2. Opening of hydraulic and natural fractures due presence of weak layer (upper figure) and tough (bottom figure) layer on the 2- and 4-layer of hydraulic fracture path.

In a third case, the tougher/weaker zone is in the fourth and fifth layers (in Figure 5.11). In this case, maximum net pressure, due to boundary effects, is reached at different times and at different magnitudes. Weak zone (red line) show at 18 minutes the effect of lower boundary (Figure 5.12 upper). Net pressure is kept almost constant until the upper boundary is reached at 74 seconds. Then, the net pressure drop is smaller than the base case as the propagation is faster in the wing than the other before reaching the intersection with natural fracture (140 seconds). On the other hand, tough zone (green line) show boundary effects at about 43 seconds because of the small height of the fracture (Figure 5.12 bottom). From 43 seconds to 100 seconds, the higher net pressure drop is observed because the fracture is propagating in three layers in one wing and in 5 layers in the other wing. Intersection effect is felt at around 100 seconds. Fracture propagation is mainly in the direction of the natural fracture showing an increase of net pressure response.

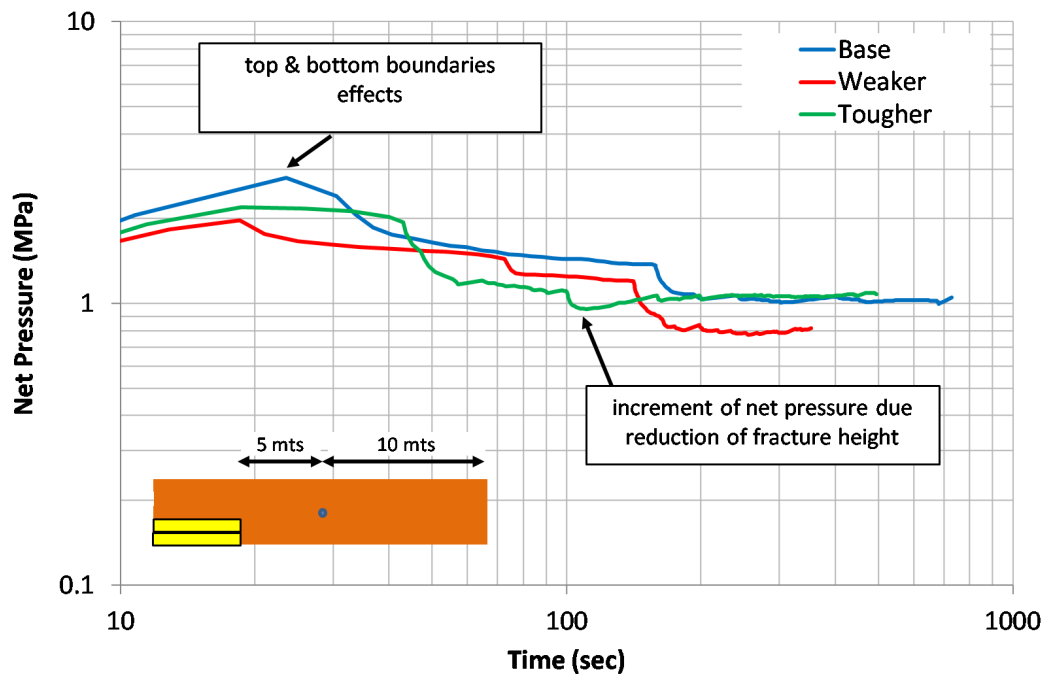


Figure 5.11: Case 3. Net pressure response when tougher/weaker layer is 4- and 5- layer. Weak layer shows lower net pressure drop and tough layer shows faster propagation in the other direction.

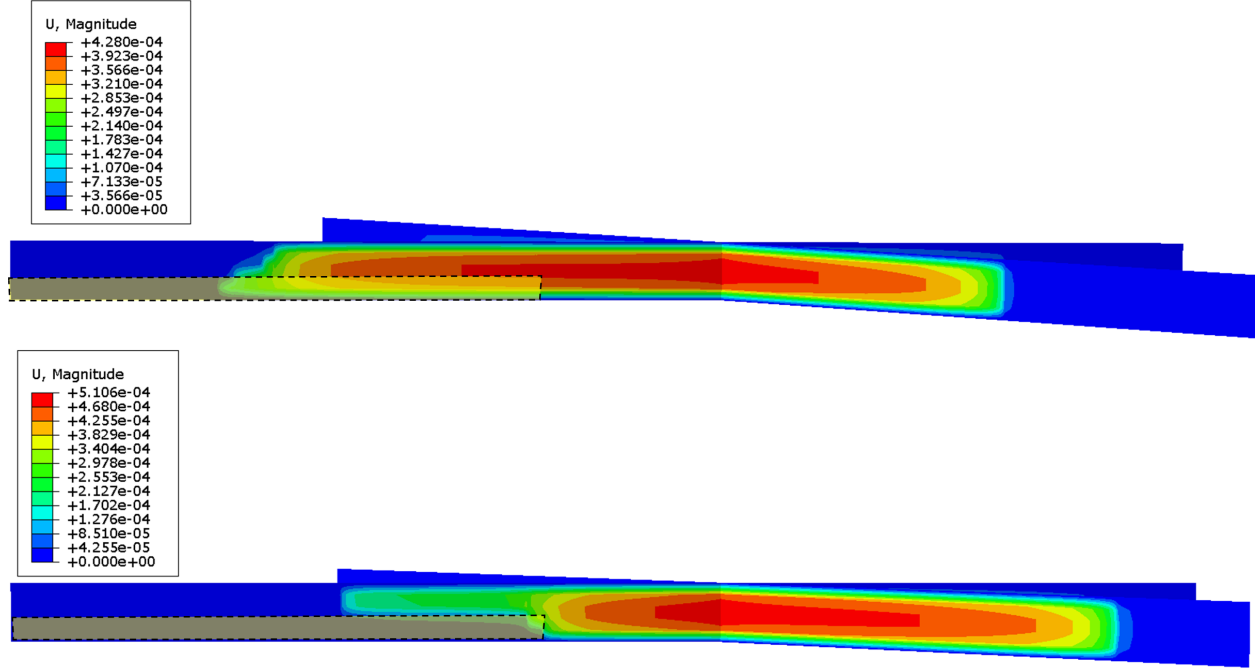


Figure 5.12: Case 3. Opening of hydraulic and natural fractures due presence of weaker (upper figure) and tougher (bottom figure) layer on the 4- and 5-layer of hydraulic fracture path.

5.5 Conclusions

The presence of natural fractures in many unconventional reservoirs, and their interaction with induced hydraulic fractures is well known and well documented in the literature. Although these fractures are mostly fully cemented with the diagenetic material, due to their weakness, they can play a significant role in forming complex fracture geometries. Here, a workflow to simulate three- dimensional simulation to model hydraulic fracture propagation through natural fractures is presented, which uses coupled fluid flow and cohesive element methods. A methodology to derive cohesive properties of rock and cemented natural fractures from a semi-circular bending test is explained. Verification of a single hydraulic fracture and its interaction with a single natural fracture is presented. Then, simulations with changes of rock properties in both hydraulic and natural fracture are shown. Net pressure response identifies changes in rock properties in horizontal and vertical direction. Also, identify changes

of propagation direction. Cases testing changes in vertical layers were analyzed. Results show that net pressure can identify changes when hydraulic fracture diverts in another path different to the maximum horizontal stress. We observed when only one of the five layers is weaker or tougher than the others; the net pressure response does not change significantly. However, tougher layer case shows a little higher pressure drop before and after reaches the intersection. Beyond this point, the net pressure increases until stabilized with the values of the weaker layer case. Contour plots show a little sharper tip fracture for the weaker layer case due propagation in this layer moves a little bit faster than the tougher case. We can highlight that in this case the layer with different rock properties represent 20 percent of the total height of the layer there is no significant change in net pressure response. For the case where the tougher/weaker layer represents 40 percent of the total fracture height with interlayering with other regular layers, we observed that tougher layer arrests the opening of the fracture in the direction of the tougher layer and promote the opening in the direction where the intersection is located. Net pressure starts to decrease once the tougher layer is detected but and there is not big jump once reaches the intersection because the increase of the net pressure due tougher layer is compensating with a decrease of changes of direction of propagation. For the weaker layer case, it can notice a higher net pressure drop due the faster propagation of the fracture in these layers. Contour plots show flat fracture tip due the weaker layers are interlayering with the regular layers. For the case when tougher/weaker layers that represent 40 percent of the total fracture height are in the bottom layers, we observed that tougher layer case that fracture propagation is not completely arrested in the direction. Moreover, there is fracture propagation above the tougher layer but with lower fracture width and fracture propagation occurs mainly propagates in the other direction where the intersection is located. For the weaker layer case, fracture propagation is mainly in the weaker layers and propagation in the natural fracture is limited.

5.6 References

- Abbaszadeh, M., Takano, Osamu, Y., Hiroshi, S., Tatsuo, Yazawa, N., Sandria, F., Zamora Guerrero, D., and Rodriguez de la Garza, F., 2003, Integrated geostatistical reservoir characterization of turbidite sandstone deposits in Chicontepec Basin, Gulf of Mexico. Society of Petroleum Engineers.
- Atkinson, B. K., and Meredith, P. G., 1987, Experimental Fracture Mechanics Data for Rocks and Minerals, Fracture Mechanics of Rock, 477525, ISBN: 978-0-12-066266-1 published by Elsevier.
- Barenblatt, G. I., 1962, The mathematical theory of equilibrium cracks in brittle fracture (in Advances in applied mechanics 7 (1): 55-129.
- Clifton, Rodney J and Abou-Sayed, Ahmed S, 1981, A variational approach to the prediction of the three-dimensional geometry of hydraulic fractures. Society of Petroleum Engineers.
- Daneshy, A Ali, 2009, Factors controlling the vertical growth of hydraulic fractures. Society of Petroleum Engineers.
- Dean, Rick H and Schmidt, Joseph H, 2009, Hydraulic-fracture predictions with a fully coupled geomechanical reservoir simulator (in Spe Journal 14 (04): 707-714.
- Dugdale, D. S., 1960, Yielding of steel sheets containing slits (in Journal of the Mechanics and Physics of Solids 8 (2): 100-104.
- Geertsma, J. and De Klerk, F., 1969, A rapid method of predicting width and extent of hydraulically induced fractures (in Journal of Petroleum Technology 21 (12): 1,571-1,581.
- Gonzalez-Chavez, M. A., Dahi-Taleghani, A., and Olson, J. E., 2015, A Cohesive Model for Modeling Hydraulic Fractures in Naturally Fractured Formations. Society of Petroleum Engineers.
- Griffith, A. A., 1921, The phenomena of rupture and flow in solids (in Philosophical transactions of the royal society of london. Series A, containing papers of a mathematical or physical character 221: 163-198.
- Gu, Hongren and Siebrits, Eduard, 2006, Effect of formation modulus contrast on hydraulic fracture height containment. Society of Petroleum Engineers.
- Khristianovic, S. and Zheltov, Y., 1955, Formation of vertical fractures by means of highly viscous fluids. Vol. 2, 579-586.
- Mack, M. G. and , N. R., 2000, Mechanics of hydraulic fracturing (in Reservoir stimulation: 6-1.
- Nolte, K. G. and Smith, M. B., 1981, Interpretation of fracturing pressures (in Journal of Petroleum Technology 33 (09): 1,767-1,775.

- Nordgren, R. P., 1972, Propagation of a vertical hydraulic fracture (in Society of Petroleum Engineers Journal 12 (04): 306-314.
- Perkins, T. K. and Kern, L. R., 1961, Widths of Hydraulic Fractures. JPT: 937-49, SPE-89-PA. Journal of Petroleum Technology.
- Sierra, R., Tran, M. H., Abousleiman, Y. N., and Slatt, R. M., 2010, Woodford Shale mechanical properties and the impacts of lithofacies. 1-10.
- Simonson, ER, Abou-Sayed, AS, and Clifton, RJ, 1978, Containment of massive hydraulic fractures (in Society of Petroleum Engineers Journal 18 (01): 27-32.
- Smith, MB, Bale, AB, Britt, LK, Klein, HH, Siebrits, E, and Dang, X, 2001, Layered modulus effects on fracture propagation, proppant placement, and fracture modeling. Society of Petroleum Engineers.
- Teufel, Lawrence W and Clark, James A, 1984, Hydraulic fracture propagation in layered rock: experimental studies of fracture containment (in Society of Petroleum Engineers Journal 24 (01): 19-32.
- Thiercelin, M., Jeffrey, R. G., and Naceur, K. B., 1989, Influence of fracture toughness on the geometry of hydraulic fractures (in SPE Production Engineering 4 (04): 435-442.
- Wang, H, Liu, H, Wu, HA, and Wang, XX, 2015, A 3D numerical model for studying the effect of interface shear failure on hydraulic fracture height containment (in Journal of Petroleum Science and Engineering 133: 280-284.
- Wang, H, Liu, H, Wu, HA, Zhang, GM, and Wang, XX, 2012, A 3D Nonlinear Fluid-solid Coupling Model of Hydraulic Fracturing for Multilayered Reservoirs (in Petroleum Science and Technology 30 (21): 2273-2283.
- Warpinski, Norman R, Schmidt, Richard A, and Northrop, David A, 1982, In-situ stresses: the predominant influence on hydraulic fracture containment (in Journal of Petroleum Technology 34 (03): 653-664.
- Zhang, G. M., Liu, H., Zhang, J., Wu, H. A., and Wang, X. X., 2010, Three-dimensional finite element simulation and parametric study for horizontal well hydraulic fracture (in Journal of Petroleum Science and Engineering 72 (3): 310-317.

Chapter 6

Conclusions and Recommendations

6.1 Summary

The presence of natural fractures in many unconventional reservoirs, and their interaction with induced hydraulic fractures is widely known in the oil and gas industry. Although these fractures are mostly fully cemented with diagenetic material, due to their weakness, they can play a significant role in change fracture pattern geometry. Here, a workflow to simulate hydraulic fracture propagation through a network of natural fractures was presented that uses coupled fluid flow and cohesive element methods. The methodology derived in this dissertation explains how to obtain cohesive parameters from loading curves obtained in routine semicircular bending tests for any field when laboratory data is available. The simulations have been implemented in a two-dimensional model (plane strain geometry) and three-dimensional planar geometries. Here, it is necessary to remark about the increase of computational cost for two- and three-dimensional models that might make it difficult to simulate large models with a significant number of fractures due the high refinement required in the cracks. Both hydraulic and natural fractures are modeled using cohesive elements. The results show the strong effect of differential stress and orientation of natural fractures on the induced fracture geometry. One of the differences of modelling fracture intersection using cohesive zone methods in comparison to LEFM is partial opening of both fractures under different circumstances, although like LEFM, the fracture will eventually propagate in the direction leads to more energy release rate.

Linear Elastic Fracture Mechanics (LEFM) has been very successful in describing the mechanics of fracture in brittle rocks, however, the success story has not repeated in the case of soft rocks. LEFM may not be the best tool to deal with problems such as soft shale rocks, and rock with ductile behavior under high temperature and high-pressure conditions in the subsurface. Additionally, LEFM neglects the details in the fracture process zone as it lumps all effects into the fracture tip stress singularity.

Net pressure response of fracture jobs is different when hydraulic fracture geometry is created in heterogeneous basins. Results show that initially negative and then positive slope in net pressure plot in heterogeneous reservoirs is not necessarily corresponding to uncontrolled or controlled height growth that is expected from Nolte-Smith analysis but probably is because propagation is not occurring in a planar path.

Results show that in addition to toughness ratio of the rock and cements inside the natural fractures and intersection angle of fractures, the ductility of the diagenetic cement inside natural fractures could have a significant effect in determining if the hydraulic fracture diverts into the natural fracture or not. Also, it is showed that toughness of the cement may be more significant in determining if the hydraulic fracture can continue its growth along a natural fracture or not. For instance, the hydraulic fracture will be arrested when the tensile strength of the natural crack is much lower than the tensile strength of the rock and only fracture widening may occur when the hydraulic fracture intersects a natural crack. On the other side, the asymmetric opening of the hydraulic fracture will be observed when the tensile strength of the crack is higher than the tensile strength of the rock.

Generally, three possibilities might occur while hydraulic fracturing in a naturally fractured reservoir: crossing, diverting, or offsetting. Such occurrences are strongly influenced by rock and fracture cement strength as well as in-situ stress direction relative to the pre-existing natural fractures (which determines approach angle between hydraulic and natural fracture). Fracture opening displacement and fluid pressure profiles for those cases were explained.

The use of CZM could address current limitations in simulations of hydraulic fracturing in naturally fractured reservoirs. For instance, the cohesive models are slower than LEFM methods due to the nonlinear nature of the cohesive laws for fracture initiation and propagation. The main drawbacks of these methods are their inability to predict the fracture path and the mesh dependency of their parameters. Cohesive zone methods due to the nature of this method require elements with certain size that make simulations in different length scales complicated and meaningless as cohesive parameters are also a function of element size. On the other hand, CZM has the advantages to predefine fracture path allowing the study of different setups of natural fractures that hydraulic fracture might be found during a fracture job. Additionally, traction-separation law (TSL) of CZM can be modeled in a different way to represent rocks with ductile behavior.

More efforts need to be undertaken to understand better when/where/how CZM can be applicable in fracture jobs in the presence of natural fractures. In the next section, a list of possible future works to continue based on the research of this dissertation is included.

6.2 Recommendations for Future Works

The following recommendations are made for possible future research about hydraulic fracture treatments in presence of natural fractures:

- Study that includes compressible injection fluid. Reservoir with low reservoir pressure needs hydraulic fracture with compressible injection fluids such as N_2 or CO_2 . Study of compressible injection fluids might help to define better the injection fluid for use in the presence of natural fractures.
- Study that includes non-Newtonian injection fluids. The combination of proppant, high fluid viscosity, and high pumping injection might change the properties of the injected fluid during the fracture job. Then, better approach can be obtained studying how

rheology of fluids might change in the function of injection pumping in heterogeneous basins.

- Study that includes non-linear natural fracture paths. Ductility of the material contained inside the natural fracture, and anisotropic in-situ stress might influence in the creation of non-linear natural fractures.
- Study that includes proppant crash during a fracture job. The integrity of proppant material might be affected during a fracture job causing heterogeneous proppant concentration through the geometry of the hydraulic fracture.

Appendix: Letters of Permission to Use Published Material

The Permissions from SPE publishing are presented in the following pages:

Order Completed

Thank you very much for your order.

This is a License Agreement between Miguel A Gonzalez-Chavez ("You") and Society of Petroleum Engineers ("Society of Petroleum Engineers"). The license consists of your order details, the terms and conditions provided by Society of Petroleum Engineers, and the [payment terms and conditions](#).

[Get the printable license.](#)

License Number	3867891320061
License date	May 14, 2016
Licensed content publisher	Society of Petroleum Engineers
Licensed content publication	SPE Proceedings
Licensed content title	A Cohesive Model for Modeling Hydraulic Fractures in Naturally Fractured Formations
Licensed content author	Miguel Gonzalez-Chavez, Louisiana State University; Arash Dahi Taleghani, Louisiana State University; Jon Edward Olson, University of Texas At Austin et al
Licensed content date	2015
Type of Use	Thesis/Dissertation
Requestor type	author of the original work
SPE member	yes
SPE member number	3006261
Format	electronic
Portion	full article
Will you be translating?	no
Distribution	1
Order reference number	None
Title of your thesis / dissertation	MODELLING HYDRAULIC FRACTURING PROPAGATION IN HETEROGENEOUS RESERVOIRS USING COHESIVE ZONE METHODS
Expected completion date	Aug 2016
Estimated size (number of pages)	100
Total	0.00 USD

[ORDER MORE...](#)

[CLOSE WINDOW](#)

Copyright © 2016 [Copyright Clearance Center, Inc.](#) All Rights Reserved. [Privacy statement](#). [Terms and Conditions](#).
Comments? We would like to hear from you. E-mail us at customercare@copyright.com

Unconventional Resources Technology Conference (URTeC) ©2015, reprinted by permission of URTeC, whose permission is required for further use.

Gonzalez-Chavez, M. A., Puyang, P., and Dahi-Taleghani, A., 2015, From Semi-Circular Bending Test to Microseismic Maps: An Integrated Modeling Approach to Incorporate Natural Fracture Effects on Hydraulic Fracturing. Society of Petroleum Engineers.

From: Miguel A Gonzalez-Chavez [<mailto:mgonz19@lsu.edu>]
Sent: Monday, April 18, 2016 5:48 PM
To: Urtec
Subject: request written permission to use my URTEC paper in my dissertation

To whom it may concern,

I'm author of the spe paper no 178544-MS with title "From Semi-Circular Bending Test to Microseismic Maps: An Integrated Modeling Approach to Incorporate Natural Fracture Effects on Hydraulic Fracturing".

I want to include this paper as a chapter of my dissertation and I tried to request written permission in Onepetro. However, the website mentioned that "Copyright is not held by SPE" and that I need to contact the meeting conference where I presented the paper.

I'll appreciate if you can tell me what I need to do to obtain the written permission.

Thanks in advance

Best regards,

Miguel Gonzalez-Chavez



Mon 4/25/2016 7:51 AM

Paula Sillman <psillman@aapg.org>

Re: request written permission to use my URTEC paper in my dissertation

To: Miguel A Gonzalez-Chavez

 You replied to this message on 5/14/2016 7:11 PM.

[EmailTranslator V1.1](#)

[+ Get more add-ins](#)

Dear Mr. Gonzalez-Chavez,

Thank you for your past participation in the URTEC meeting.

According to the URTEC Royalty Free Rights, you have permission to reproduce your URTEC paper as long as proper copyright acknowledgment is included. Your URTEC paper can be included in your dissertation as long as the following copyright acknowledgment is included in the following format:

[Unconventional Resources Technology Conference \(URTEC\) © 2015, reprinted by permission of URTEC, whose permission is required for further use.](#)

You will also need to put the full citation for the URTEC paper in your bibliography.

Thank you again for participating in URTEC and we hope you will be able to be a presenter at future meetings.

Kind regards,
Paula

—
Paula Sillman
AAPG Technical Publications Assistant Team Lead

Vita

Miguel Alejandro Gonzalez-Chavez, son of Socorro Chavez-Gomez and Roberto Gonzalez, was born in Mexico, Distrito Federal in 1977. He joined Craft and Hawkins Department of Petroleum Engineering geomechanics research group at LSU as a Ph.D. student in Fall 2011 where he started his research under the supervision of Dr. Arash Dahi Taleghani.

Before joining LSU, he worked in a National Mexican Oil company, Petroleos Mexicanos, where he was selected to perform doctoral studies. He holds a B. S. and M. S. degrees in Petroleum Engineering at National University Autonomous of Mexico. He is currently with Petroleos Mexicanos working at Mexico City.

He received first place award in the Student Contest from Petroleum Engineering Department at LSU (2015), and third place in East Regional SPE Student Contest (2015). He is currently a member of Society of Petroleum Engineers (SPE), American Rock Mechanics Association chapter LSU (ARMA), College of Mexican Petroleum Engineers (CIPM), and Association of Mexican Petroleum Engineers (AIPM).

He is married to Norma Rivas-Osollo, and they have two children: Alejandra (5 years old) and Miguel (4 years old).

Miguel Alejandro Gonzalez-Chavez is expected to receive his Doctor of Philosophy degree at the 2016 Summer Commencement.